Universidade de São Paulo
Instituto de Física

Cosmologia de Campos Escalares Taquiônicos

Fábio Chibana de Castro

Orientador: Prof. Dr. Elcio Abdalla

Dissertação de mestrado apresentada ao Instituto de Física para a obtenção do título de Mestre em Ciências

Banca Examinadora:

Prof. Dr. Elcio Abdalla (IF-USP)
Prof. Dr. Alberto Vazquez Saa (IMECC-UNICAMP)
Prof. Dr. Júlio César Fabris (CCE-UFES)

São Paulo
2017

FICHA CATALOGRÁFICA
Preparada pelo Serviço de Biblioteca e Informação
do Instituto de Física da Universidade de São Paulo

Castro, Fábio Chibana de

Cosmologia de campos escalares taquiônicos. São Paulo, 2017.

Dissertação (Mestrado) – Universidade de São Paulo. Instituto de Física. Depto. de Física Matemática

Orientador: Prof. Dr. Elcio Abdalla

Área de Concentração: Cosmologia

Unitermos: 1. Cosmologia; 2. Energia escura; 3. Matéria escura; 4. Táquions.

USP/IF/SBI-026/2017

University of São Paulo
Institute of Physics

Tachyon Scalar Field Cosmology

Fábio Chibana de Castro

Advisor: Prof. Dr. Elcio Abdalla

Dissertation presented to the Institute of Physics of the University of São Paulo in partial fulfillment of the requirements for the degree of Master of Science

Examining Commission:

Prof. Dr. Elcio Abdalla (IF-USP)
Prof. Dr. Alberto Vazquez Saa (IMECC-UNICAMP)
Prof. Dr. Júlio César Fabris (CCE-UFES)

São Paulo
2017

Acknowledgements

To Prof. Elcio Abdalla, for the trust and for giving me the opportunity to work in such a thrilling area.

To Prof. Elcio's Cosmology group, for their support, for sharing their knowledge, and for helping me out whenever possible.

To all the friends I made at the University through all these years, for the fun times and conversations.

To all my family, especially my parents, for their support and encouragement.

To my girlfriend, for her love and patience.

Resumo

Neste trabalho testamos um modelo cosmológico com uma interação entre energia escura e matéria escura, onde um campo escalar taquiônico desempenha o papel da energia escura. Para isso, desenvolvemos um código computacional que resolve as equações numericamente e vincula os parâmetros cosmológicos e, assim, comparamos os resultados do modelo taquiônico interagente com os de outros candidatos à energia escura. Nossas análises mostram que o modelo, de fato, consegue explicar os dados observacionais, além de possuir propriedades cosmológicas interessantes, mas apresenta dificuldades quando comparado a outros modelos de energia escura.

Palavras-chave: Cosmologia. Energia Escura. Matéria Escura. Táquion.

Abstract

In this work we test a cosmological model with an interaction between dark energy and dark matter, where a tachyon scalar field plays the role of dark energy. With that in mind, we developed a numerical code that solves the background equations and extracts the cosmological parameters and we compared the results of the interacting tachyon model with those of other dark energy candidates. Our results show that the model indeed explains the observational data and has interesting cosmological properties, but might face challenges when compared to other dark energy candidates.

Keywords: Cosmology. Dark Energy. Dark Matter. Tachyon.

Acronyms

6dF 6dF Galaxy Survey. 90

AIC Akaike Information Criterion. 86, 87

BAO baryon acoustic oscillations. 44

BIC Bayesian Information Criterion. 87

BOSS Baryon Oscillation Spectroscopic Survey. 91

BOSS-CMASS Baryon Oscillation Spectroscopic Survey's CMASS. 91

BOSS-LOWZ Baryon Oscillation Spectroscopic Survey's LOWZ. 91

CC cosmic chronometer. 88

CDM cold dark matter. 30

CMB cosmic microwave backgroud. 38

DE dark energy. 31

FLRW Friedmann-Lemaître-Robertson-Walker. 21

GCG generalized Chaplygin gas. 68

HST Hubble Space Telescope. 89

IDE Interacting Dark Energy. 59

ISW integrated Sachs-Wolfe. 40

ITM Interacting Tachyon Model. 73

JLA Joint Light-curve Analysis. 39, 89

MCMC Monte Carlo Markov Chain. 86

PDF probability density function. 81

Planck15 Planck Collaboration 2015 Data Release. 92

SDSS-II Sloan Digital Sky Survey. 89

SDSS-MGS Sloan Digital Sky Survey's Main Galaxy Sample. 90

SNIa type Ia supernova. 37

SNLS Supernova Legacy Survey. 89

UDM Unified Dark Matter. 67

WFC3 Wide Field Camera 3. 36, 37

WiggleZ WiggleZ Dark Energy Survey. 91

Contents

Chapter 1

Introduction

Cosmology is the branch of physics that studies the origin and development of the universe, employing both observational astronomy and particle physics concepts. It is based on the cosmological principle which states that, on large scales, the universe is homogeneous and isotropic.

Modern cosmology is described by the Big Bang theory. The universe started as a tiny spot, very dense and hot. As it expanded it cooled down, forming nuclei in a process called *Big Bang nucleosynthesis*.

After the Big Bang, the history of the universe may be divided into four epochs: a primordial inflationary period, when the universe expanded at a stunning rate, followed by radiation- then a matter-dominated epoch, and recently it entered a late-time accelerated expansion phase.

For the past couple of decades, one of the most intriguing problems of cosmology has been the nature of recently accelerated phase, which cannot be explained within the standard framework of general relativity and Standard Model of particle physics. Extra degrees of freedom are needed. One can attribute these extra degrees of freedom to a new, exotic form of matter, generically called *dark energy* (DE). On the other hand, the extra degrees of freedom could also have a geometrical origin, arising from a modification to the theory of gravitation that yields general relativity as a particular limit. The first approach has been the standard one for a while now, although the latter has also received a fair amount of attention, especially in recent years.

Dark energy is a very active research area, gathering efforts from theorists and experimentalists alike. A number of astrophysical experiments are undergoing or planned to be launched soon and a plethora of models have been proposed in the literature throughout the years.

The simplest cosmological model capable of explaining the observations assumes that Einstein's cosmological constant Λ is the source of dark energy. The cosmological constant was originally introduced by Einstein as an attempt to keep the universe static but was abandoned after Hubble's observations of the expansion of the universe. In the context of DE, Λ is equivalent to an emergent smooth fluid, with negative pressure and whose equation of state is $w = -1$.

Hence in the standard model, so-called ΛCDM, the universe's energy budget is divided between Λ ($\sim 70\%$), cold dark matter, CDM, ($\sim 25\%$), and ordinary baryonic matter ($\sim 5\%$), with a negligible fraction of relativist matter (photons and neutrinos).

Despite its success in reproducing the current observational data, the cosmological constant faces important theoretical challenges such as the fine-tuning and the coincidence problems. Therefore, we are invited to explore generalization of Λ usually considering dynamical dark energy models. In this work, we discuss some of these alternatives. Examples of dynamical DE candidates include fluids with varying equation of state, scalar fields with slow-roll potentials, and coupled dark energy models.

Here we place special emphasis on the tachyon scalar field. Our main goal is to analyze how well a coupled dark energy model, where the tachyon interacts with cold dark matter, can reproduce the cosmological observations, and compare the results among different DE candidates.

The rest of the work is arranged as follows. In Chapter 2, we introduce the most relevant cosmological concepts that will be used throughout the following chapter, namely, we introduce the homogeneous and isotropic space-time and the Friedmann equations, discuss briefly the matter species the form the current universe and define the relevant cosmological distances. In Chapter 3 we present some candidates to dark energy, discussing the cosmological constant, parameterizations of the equation of state

for DE, scalar field models and coupled dark energy proposals. Cosmological applications of the tachyon scalar field are presented in Chapter 4, where we also formulate the interacting tachyon model. In Chapter 5 the methods of parameter estimation and data analysis, together with the data sets, are introduced. Our constraints on the dark energy models and the comparison between them are also presented in this chapter. Finally, in Chapter 6 we present our conclusions and briefly discuss possible paths one could take to improve our results.

Chapter 2

Basics of cosmology

In this chapter, we develop the basic tools to understand the expansion history of the universe, such as the FLRW metric and the Friedmann equations. We also itemize the components of the universe. The concept of distance is crucial in an expanding universe, hence we deal with it by the end of the chapter.

2.1 Einstein equations

The key point of General Relativity is that since gravity affects all objects in the same way, i.e. it is universal, it should be identified with something equally universal: the geometry of space-time.

The notions of spatial and temporal separations are not invariant by themselves in the relativity theory. What is invariant is the combination,

$$\mathrm{d}s^2 = g_{\mu\nu}(x)\,\mathrm{d}x^\mu\,\mathrm{d}x^\nu\,, \tag{2.1}$$

where $\mu, \nu = 0, 1, 2, 3$ and repeated indices are summed over. The geometric information is encapsulated in the object $g_{\mu\nu}$, the so-called *metric tensor*. It is used to measure distances between events and, in curved space-times, it depends on the coordinates x^μ. In this work, we adopt the metric signature $(-, +, +, +)$.

Just as Maxwell's equations dictate the behavior of electric and magnetic fields

through second-order differential equations, we expect the equations that govern the geometry of space-time to be of second-order on the metric field. The object that contains all the information about the curvature is called Riemann curvature tensor and is defined as [1]

$$R^{\rho}{}_{\sigma\mu\nu} = \partial_\mu \Gamma^{\rho}_{\nu\sigma} - \partial_\nu \Gamma^{\rho}_{\mu\sigma} + \Gamma^{\rho}_{\mu\lambda}\Gamma^{\lambda}_{\nu\sigma} - \Gamma^{\rho}_{\nu\lambda}\Gamma^{\lambda}_{\mu\sigma} \tag{2.2}$$

where $\partial_\mu \equiv \partial/\partial x^\mu$. The symbol $\Gamma^{\sigma}_{\mu\nu}$ is called Christoffel symbol and is used to properly define the concept of derivative in a covariant way in curved geometries. Its explicit form in terms of $g_{\mu\nu}$ is

$$\Gamma^{\sigma}_{\mu\nu} = \frac{1}{2} g^{\sigma\rho} \left(\partial_\mu g_{\nu\rho} + \partial_\nu g_{\mu\rho} - \partial_\rho g_{\mu\nu} \right).$$

Thus the Riemann tensor (2.2) contains second derivatives of the metric. To condense the dynamics of the curvature in an invariant object, i.e. a scalar, we can take traces of the $R^{\rho}{}_{\sigma\mu\nu}$. First, we get the Ricci tensor

$$R_{\mu\nu} = R^{\lambda}{}_{\mu\lambda\nu},$$

while the Ricci scalar is obtained contracting the remaining indices with the inverse metric

$$R = R^{\mu}{}_{\mu} = g^{\mu\nu} R_{\mu\nu}.$$

Now we are in a position to define the simplest action that is scalar and has two derivatives of the metric,

$$S = \int \mathrm{d}x^4 \sqrt{-g} R, \tag{2.3}$$

where we include the determinant of the metric $\sqrt{-g}$ so the integration measure is properly defined in curved space-times. The action (2.3) is called Einstein-Hilbert action. When we extremize it with respect to the metric we get the equations of

motion for $g_{\mu\nu}$, namely, the Einstein equations in the vacuum [1]

$$R_{\mu\nu} - \frac{1}{2}Rg_{\mu\nu} = 0. \tag{2.4}$$

But the universe is not empty. So we should consider the following generalization,

$$S = \int \mathrm{d}x^4 \sqrt{-g}\frac{R}{16\pi G} + S_M, \tag{2.5}$$

where S_M is the action for matter, and the normalization factor $(16\pi G)^{-1}$ ensures that in the non-relativistic limit we go back precisely to the Newtonian theory, with the familiar universal gravitational constant G. Now, extremizing the new action (2.5), we find

$$R_{\mu\nu} - \frac{1}{2}Rg_{\mu\nu} = 8\pi G T_{\mu\nu}, \tag{2.6}$$

where $T_{\mu\nu}$ is the energy-momentum tensor, defined as

$$T_{\mu\nu} \equiv -\frac{2}{\sqrt{-g}}\frac{\delta S_M}{\delta g^{\mu\nu}}. \tag{2.7}$$

The equations of motion (2.6) are the ones we were looking for. They relate the curvature of space-time, on the LHS, with the energetic content, on the RHS. Given the symmetry properties of the Riemann tensor (2.2), the LHS of Eq. (2.6) satisfies

$$\nabla^\mu \left(R_{\mu\nu} - \frac{1}{2}Rg_{\mu\nu} \right) = 0, \tag{2.8}$$

which is called Bianchi identity [1], leading to the conservation of the energy-momentum tensor $\nabla^\mu T_{\mu\nu} = 0$.

2.2 Homogeneous and isotropic universe

Now let us find out how the universe evolves. The rules are set: Einstein's equations will dictate how geometry and energy are linked. All we need to do now is define the

[1] For the full derivation of Eq.(2.4) from the action (2.3) see Ref. [2].

metric that describes our universe and identify the source of energy that fills it up.

Cosmological models are based on the Copernican principle, which states that neither Earth nor the Sun are in favored positions in the cosmos. In other words, the principle argues that we, as humans, are not privileged observers of the universe. It is related to two important properties: isotropy and homogeneity. The former means that space looks the same in every direction, i.e. there is no privileged direction, while the latter means that the universe is the same in every spot.

Isotropy and homogeneity are not necessarily related since one can have a geometric object that is isotropic but not homogeneous. However, if space is isotropic on every single point, then it has to be homogeneous. Conversely, if it is isotropic at one point but is also homogeneous, it has to be isotropic everywhere.

Observations of the cosmic microwave background show that its temperature is roughly the same in every direction in the sky (the fluctuations are of the order $\sim 10^{-5}$) indicating the isotropy. On top of that, we have no reason to believe we are in a privileged position (Copernican principle). Hence we assume the homogeneity and isotropy of the universe.

Of course, these properties only apply at large-scales. The surface of Earth is not the same as, say, the center of a black hole, or the empty intergalactic medium. Nevertheless, in scales larger than 100 Mpc (where $1\,\mathrm{pc} = 3.09 \times 10^{16}\,\mathrm{m} = 3.26\,\mathrm{ly}$), the universe becomes homogeneous to a large level.

The inhomogeneities and irregularities we observe in the local universe, such as stars and galaxies were seeded as small deviations from homogeneity at early epochs, and have grown in time through gravitational instability.

2.2.1 FLRW metric

In this section we will state the concepts of homogeneity and isotropy in mathematical language, defining the FLRW metric, and we'll apply it to the Einstein equations.

In a four-dimensional homogeneous and isotropic space-time the line element (2.1)

becomes [2]

$$\mathrm{d}s^2 = -\,\mathrm{d}t^2 + a^2(t)\left[\frac{\mathrm{d}r^2}{1-Kr^2} + r^2\left(\mathrm{d}\theta^2 + \sin^2\theta\,\mathrm{d}\phi^2\right)\right], \tag{2.9}$$

and the corresponding $g_{\mu\nu}$ is called the Friedmann-Lemaître-Robertson-Walker (FLRW) metric. The function $a(t)$ is a scale factor with cosmic time t, usually normalized as $a(t_0) \equiv a_0 = 1$, where t_0 is the age of the universe. The index 0 always refers to the present value of the quantity carrying it. The constant K gives the curvature of the space-time, with $K = +1, -1, 0$ corresponding to closed, open, and flat geometries, respectively. The radial coordinates r, θ and ϕ are known as comoving coordinates. A freely moving particle comes to rest in these coordinates. In addition to the cosmic time t, it is useful to also introduce the conformal time η,

$$\eta \equiv \int \mathrm{d}t\, a^{-1}.$$

Sometimes it is convenient to write the metric (2.9) in the following form:

$$\mathrm{d}s^2 = -\,\mathrm{d}t^2 + a^2(t)\left[\mathrm{d}\chi^2 + f_K^2(\chi)\left(\mathrm{d}\theta^2 + \sin^2\theta\,\mathrm{d}\phi^2\right)\right], \tag{2.10}$$

where

$$f_K(\chi) = \begin{cases} \sin\chi, & K = +1, \\ \chi, & K = 0, \\ \sinh\chi, & K = -1. \end{cases}$$

Now we must plug Eq. (2.9) into Einstein's equations (2.6) to derive the Friedmann equations relating the scale factor to the energy-momentum of the universe. The

[2] See Carroll's book [2] for a derivation of the metric (2.9) from a maximally symmetric space-time.

curvature terms will be given by

$$\begin{aligned} R_0^0 &= 3\frac{\ddot{a}}{a}, \\ R_j^i &= \left(\frac{\ddot{a}}{a} + 2\frac{\dot{a}^2}{a^2} + 2\frac{K}{a^2}\right)\delta_j^i, \\ R &= 6\left(\frac{\ddot{a}}{a} + \frac{\dot{a}^2}{a^2} + \frac{K}{a^2}\right), \end{aligned} \tag{2.11}$$

where a dot denotes a derivative with respect to t. We note that the dynamics are associated with the scale factor and Einstein's equations allow us to determine $a(t)$ provided the matter content of the universe is specified. To be compatible with homogeneity and isotropy, the energy-momentum tensor usually have the form of a perfect fluid at rest in comoving coordinates [3],

$$T^{\mu}{}_{\nu} = (\rho + p)u^{\mu}u_{\nu} + p\delta^{\mu}{}_{\nu} = \mathrm{diag}(-\rho(t), p(t), p(t), p(t)). \tag{2.12}$$

where ρ is the fluid's energy density, p its the pressure, and the four-velocity u^{μ} is

$$u^{\mu} = (1, 0, 0, 0).$$

Plugging the curvature terms (2.11) and the energy-momentum tensor (2.12) into the Einstein equations (2.6) leads to the Friedmann equations,

$$H^2 \equiv \left(\frac{\dot{a}}{a}\right)^2 = \frac{8\pi G}{3}\rho - \frac{K}{a^2}, \tag{2.13}$$

$$\dot{H} = -4\pi G\left(\rho + p\right) + \frac{K}{a^2}, \tag{2.14}$$

where H is called Hubble parameter, ρ and p denote the total energy density and pressure of all species present in the universe at a given epoch. Friedmann's equations pack all the information we were seeking about the homogeneous and isotropic universe. It dictates how the scale factor dynamically changes in response to the matter content. Conversely, it determines the evolution of the species at any given era. The energy momentum tensor is conserved by virtue of the Bianchi identities (2.8), leading to the

continuity equation

$$\dot{\rho} + 3H(\rho + p) = 0. \tag{2.15}$$

Note that both Friedmann equations and the continuity equation are not independent of each other. Actually, Eq. (2.15) can be derived differentiating the first Friedmann equation (2.13) and comparing the result with (2.14). Eliminating the K/a^2 term from Eqs. (2.13) and (2.14), we obtain another useful expression,

$$\frac{\ddot{a}}{a} = -\frac{4\pi G}{3}(\rho + 3p). \tag{2.16}$$

It is also convenient to define an equation of state relating ρ and p. For cosmological fluids, this relation is usually given by

$$p = w\rho. \tag{2.17}$$

Most of the fluids we encounter in cosmological applications have constant w. Indeed, for relativistic species $w = 1/3$ whereas for non-relativistic $w = 0$. However, we can also consider species with $w = p/\rho$ varying in time, as we will see in the next chapter for dark energy.

The accelerated expansion ($\ddot{a} > 0$) occurs for $\rho + 3p < 0$, according to Eq. (2.16), which translates into the requirement $w < -1/3$. Thus we need an exotic new component with negative pressure dominating the energy balance in order to explain an accelerated expansion. To quantify the phenomena, we define the deceleration parameter

$$q = -\frac{a\ddot{a}}{\dot{a}^2} \tag{2.18}$$

which measures the rate of change of the rate of expansion.

Another useful quantity is the dimensionless density parameter,

$$\Omega = \frac{8\pi G\rho}{3H^2} = \frac{\rho}{\rho_{crit}}, \tag{2.19}$$

where $\rho_{crit} = 3H^2/8\pi G$ is the critical density. It is called "critical" because we can recast the Friedmann equation (2.13) as

$$\Omega - 1 = \frac{K}{aH^2},$$

hence the matter distribution determines the spatial geometry of our universe, i.e. K is determined by whether the density is greater or smaller than the critical value. Indeed we have:

$$\begin{aligned} &\Omega > 1 \quad \text{or} \quad \rho > \rho_c \rightarrow K = +1, \\ &\Omega = 1 \quad \text{or} \quad \rho = \rho_c \rightarrow K = 0, \\ &\Omega < 1 \quad \text{or} \quad \rho < \rho_c \rightarrow K = -1. \end{aligned}$$

Observations have shown that the current universe is very close to a spatially flat ($\Omega \approx 1$) [4], which is actually a natural result from the inflationary theory of the early universe [5]. Hence, for the rest of this work, we will only consider flat cosmologies ($K = 0$), unless otherwise stated.

2.2.2 The evolution of the universe filled with perfect fluids

Now let's see how the universe evolves with time. The continuity equation (2.15) can be easily integrated, taking the form

$$\rho(a) = \rho_0 \exp\left\{ - \int \frac{\mathrm{d}a}{a} 3\left[1 + w(a)\right] \right\} \tag{2.20}$$

where we used the definition of the equation of state (2.17) and ρ_0 is the current value of the density. Let us consider the evolution of the universe filled with a single perfect fluid with a constant equation of state parameter. Solving the Einstein equations given

in Eqs. (2.13) and (2.14), we obtain

$$H = \frac{2}{3(1+w)t}, \tag{2.21}$$

$$a(t) \propto t^{\frac{2}{3(1+w)}}, \tag{2.22}$$

$$\rho \propto a^{-3(1+w)}, \tag{2.23}$$

except for an integration constant that can be ignored for the time being. We note that the above solution is valid for $w \neq -1$, and we deal with this possibility soon. As we stated previously, the radiation-dominated universe corresponds to $w = 1/3$, whereas the dust-dominated universe to $w = 0$. In these cases we have

$$\text{Radiation:} \quad a(t) \propto t^{1/2}, \quad \rho \propto a^{-4},$$

$$\text{Dust:} \quad a(t) \propto t^{2/3}, \quad \rho \propto a^{-3}.$$

Both correspond to a decelerated expansion of the universe. The dependence of these energy densities on the scale factor can be understood on fairly simple physical grounds. For non-relativistic dust, its mass m is much larger than its momentum, so $\rho_{dust} = E/V \sim m/V \sim a^{-3}$, since the volume V scales with a^{-3}. On the other hand, for relativistic matter, there is also the dependence on the wavelength λ of the radiation, which gets stretched by the expansion. The combined effect leads to $\rho_{rad} \sim a^{-4}$. The amount of stretch can be quantified by the redshift

$$z \equiv \frac{\lambda_0}{\lambda} - 1 = \frac{1}{a} - 1 \tag{2.24}$$

where λ is the originally emitted wavelength and λ_0 is the observed one. Note that the redshift, just like the scale factor, can also be used to keep track of time. Today, $z = 0$ and at the early universe $z \to \infty$.

In order to explain the current acceleration of the universe, we require an exotic energy dubbed "dark energy" with an equation of state satisfying $w < -1/3$. This condition means that we essentially require a large negative pressure in order to give

rise to an accelerated expansion. An interesting and very simple case occurs when ρ is constant. From Eq. (2.15), the energy density ρ is constant for $w = -1$. In this case, the Hubble rate is also constant from Eq. (2.13) and the scale factor evolves as

$$a \propto e^{Ht}.$$

The fluid with negative pressure and constant energy density can be identified as the cosmological constant Λ, as we will see in the next section.

In the general case, the universe is filled with several components. Inspired by Eq. (2.19), we thus define the fractional density parameter

$$\Omega_i = \frac{8\pi G\rho_i}{3H^2} = \frac{\rho_i}{\rho_{crit}}, \tag{2.25}$$

for each of fluid (represented by the index i). We recast the first Friedmann equation (2.13) as

$$H(z) = H_0 \left[\sum_i \Omega_i(z)\right]^{1/2}, \tag{2.26}$$

where the summation is performed over all components. Note that in Eq. (2.25) the definition of Ω_i is not necessarily constant. The current value of the fractional density parameter is defined as

$$\Omega_i^{(0)} = \frac{8\pi G\rho_i^{(0)}}{3H_0^2} = \frac{\rho_i^{(0)}}{\rho_{crit}^{(0)}}, \tag{2.27}$$

where, as usual, quantities measured today are marked with the index (0).

2.3 Cosmic inventory

The matter species in the universe are broadly classified as relativistic particles, non-relativistic matter, and dark energy. Consider a particle with momentum $\mathbf{k}$ mass m and energy $E = \sqrt{k^2 + m^2}$, where $k \equiv |\mathbf{k}|$. The distribution function of this particle,

in equilibrium at temperature T, is

$$f(\mathbf{k}) = \frac{1}{e^{(E-\mu)/T} \pm 1} \tag{2.28}$$

where μ is the chemical potential and the Boltzmann constant is assumed to be $k_B = 1$. The plus and minus signs represent the Fermi–Dirac distribution and the Bose–Einstein distribution, respectively. Generally the distribution function f also depends on the position x, but in a homogeneous universe Eq. (2.28) only depends on $|k|$. Since the minimum volume of phase space in terms of x and k is given by $(2\pi\hbar)^3$ due to Heisenberg's principle, the number of phase space elements is $\mathrm{d}^3x\,\mathrm{d}^3k\,/(2\pi\hbar)^3$. Then, in units where $\hbar = 1$, the energy density ρ is [3]

$$\begin{aligned}\rho &= g_* \int \frac{\mathrm{d}^3k}{(2\pi)^3} E(k) f(k) \\ &= \frac{g_*}{2\pi^2} \int_m^\infty \mathrm{d}E\, \frac{\sqrt{E^2 - m^2}}{e^{(E-\mu)/T} \pm 1} E^2,\end{aligned} \tag{2.29}$$

where g_* internal degrees of freedom. On the other hand, the pressure is

$$\begin{aligned}p &= g_* \int \frac{\mathrm{d}^3k}{(2\pi)^3} \frac{kv}{3} f(k) \\ &= \frac{g_*}{6\pi^2} \int_m^\infty \mathrm{d}E\, \frac{(E^2 - m^2)^{3/2}}{e^{(E-\mu)/T} \pm 1} E^2.\end{aligned} \tag{2.30}$$

Note that since ρ and p are defined as quantities per unit volume, there is no integral over d^3x. Let us study relativistic and non-relativistic particles separately.

2.3.1 Relativistic Species

In the relativistic limit we have $T \gg m$, which corresponds to $m \to 0$ in Eqs. (2.29) and (2.30). For non-degenerate particles ($T \gg \mu$) we have

$$\rho = \begin{cases} (\pi^2/30)\, g_* T^4, & \text{(Bosons)} \\ (7/8)\,(\pi^2/30)\, g_* T^4, & \text{(Fermions)}, \end{cases} \tag{2.31}$$

$$p = \rho/3, \tag{2.32}$$

where we have used $\int_0^\infty \mathrm{d}^3x\, x^3/(e^x - 1) = \pi^4/15$ and $\int_0^\infty \mathrm{d}^3x\, x^3/(e^x + 1) = 7\pi^4/120$. We see from Eq. (2.32) that the equation of state of non-degenerate relativistic particles is $w = 1/3$, which leads, according to Eq. (2.23), to $\rho \propto a^{-4}$. Therefore, comparing with Eq. (2.31), we see that $T \propto a^{-1}$.

Photons are spin-1 particles, thus bosons, with two spin states $g_* = 2$. The relation between the temperature and chemical potential for CMB photons is constrained to be $\mu/T < 9 \times 10^{-5}$ [6]. Thus, from Eq. (2.31) we have

$$\rho_\gamma(T) = \frac{\pi^2}{15} T^4.$$

The current temperature of the CMB photons was reported to be $T_{CMB} = 2.7255(6)\,\mathrm{K}$ [7], leading to

$$\rho_\gamma^{(0)} = 4.6436 \times 10^{-34}\,\mathrm{g\,cm^{-3}}, \tag{2.33}$$

where we used the conversion factor $1\,\mathrm{K}^4 = 1.279 \times 10^{-35}\,\mathrm{g\,cm^{-3}}$. The present energy density, Eq. (2.33), corresponds to a dimensionless density parameter, Eq. (2.27),

$$\Omega_\gamma^{(0)} = 2.4721 \times 10^{-5}\, h^{-2} = 5.0451 \times 10^{-5}, \tag{2.34}$$

where $H_0 = 100\, h\,\mathrm{km\,s^{-1}\,Mpc^{-1}}$, and we used $h = 0.7$.

Neutrinos are also relativistic components, given that their masses are small, with the following properties: they have one spin degree of freedom, have anti-particles,

come in three generations (electron, muon and tau neutrinos), are fermions, and their temperature T_ν after the decoupling is related to the photon temperature T_γ via [3]

$$\frac{T_\nu}{T_\gamma} = \left(\frac{4}{11}\right)^{1/3}. \tag{2.35}$$

Using the fermionic case in Eq. (2.31), the energy density of neutrinos is given by

$$\rho_\nu = N_{eff}\frac{7\pi^2}{120}T_\nu^4 \tag{2.36}$$

where N_{eff} is the effective number of neutrino species. From Eqs. (2.35) and (2.36), we see that the energy density of neutrinos and photon are linked via

$$\rho_\nu = N_{eff}\frac{7}{8}\left(\frac{4}{11}\right)^{4/3}\rho_\gamma.$$

The sum of photons and relativistic neutrinos forms the radiation contribution to the energy budget of the universe, and the present density parameter is expressed as

$$\Omega_r^{(0)} = \frac{\rho_\gamma^{(0)} + \rho_\nu^{(0)}}{\rho_{\rm crit}^{(0)}} = \Omega_\gamma^{(0)}\left(1 + 0.2271 N_{eff}\right),$$

where $\Omega_\gamma^{(0)}$ is given by Eq. (2.34). Using $N_{eff} = 3.04$, we get

$$\Omega_r^{(0)}h^2 = 4.1788 \times 10^{-5}. \tag{2.37}$$

2.3.2 Non-relativistic species

For non-relativistic particles, i.e. $T \ll m$, Eqs. (2.29) and (2.30) become

$$\rho = g_* m\left(\frac{mT}{2\pi}\right)^{3/2}\exp\left[-(m-\mu)/T\right], \tag{2.38}$$

$$P = g_* T\left(\frac{mT}{2\pi}\right)^{3/2}\exp\left[-(m-\mu)/T\right] = \frac{T}{m}\rho. \tag{2.39}$$

These equations are valid for both bosonic and fermionic species. Note, from

Eq. (2.39), that the pressure p is suppressed by a factor $T/m \ll 1$ with respect to the energy density ρ, which means that the equation of state for non-relativistic matter is $w \approx 0$, as expected. Unlike relativistic matter, non-relativistic species cannot be described as a gas at a given temperature and zero chemical potential. Therefore, the baryon density must be measured directly, not via the temperature.

The first example of non-relativistic matter are the baryons. In cosmology, we collectively refer to nuclei and electrons as baryons, which is technically wrong and somewhat misleading, since electron are actually leptons. However, since nuclei are much more massive than electrons, for all intents and purposes all the mass is in the baryons. There are several ways to probe the baryons density in the universe. The most straightforward is to observe the baryons today in form of gas inside the galaxies. One can also infer the baryon density by analyzing the spectra of distance quasars, which gives information about the intervening hydrogen. A third method is measuring the abundance of light elements produced at the Big Bang Nucleosynthesis epoch, such as the abundance of deuterium relative to hydrogen. Finally, there is also the possibility of inferring Ω_b from CMB anisotropy measurements. From the 2015 analysis of the Planck satellite mission data combined with other low redshift measurements, the constraint on the current value of the baryon density parameter is [4]

$$\Omega_b^{(0)} h^2 = 0.02230 \pm 0.00014, \tag{2.40}$$

at the 68% confidence level. Assuming $h = 0.7$ we get $\Omega_b^{(0)} = 0.04551$ for the central value in Eq. (2.40), which means that baryons contribute with roughly 5% to the energy budget of the universe.

In addition to baryons, astrophysical observations, such as the rotation curves of galaxies, and clustering measurements, require the existence of an additional, dust-like component, that does not shine, but whose gravitational effects are measured, called dark matter. In the current paradigm, being a non-relativistic (cold) particle, it is dubbed cold dark matter (CDM). The origin of CDM has not been identified yet. Some examples of particle candidates are axions, originally introduced as a solution

to the strong CP problem, and supersymmetric particles, such as WIMPs - Weakly Interacting Massive Particles [8]. Cosmic microwave anisotropy data shows that the present abundance of dark matter is roughly 5 times larger than that of baryons. The 2015 analysis of the Planck satellite mission data combined with low-z measurements constraints the density parameter of CDM to be [4]

$$\Omega_c^{(0)} h^2 = 0.1188 \pm 0.0010$$

at the 68% confidence level. For the value $h = 0.7$ we have $\Omega_c^{(0)} = 0.2424$, so CDM contributes with around 25% of the critical energy density.

2.3.3 Dark energy

There are several direct observational shreds of evidence pointing toward the existence of something else, some other source of energy that can not be identified with matter or radiation, as we'll see in the next chapter. But for the moment, we already have a hint that baryons, cold dark matter, photons, and neutrinos are not enough. Observations of the CMB, as already mentioned, indicate that the universe is flat to a high degree, which means that the total energy density is very close to the critical value. If that is the case, from Eq. (2.19), the total sum of the energy density parameters Ω should be close to unity. However, adding up the contributions from all the components described so far totals around 30% of the critical density. The remaining 70% of the density of the universe must be in some smooth, maybe unclustered form, the so-called dark energy (DE).

2.4 The standard cosmological model

The current cosmological paradigm is known as ΛCDM model, where cold dark matter and dark energy, in the form of a cosmological constant Λ, are the dominant ingredients. The expansion history is given by the Friedmann equation (2.26) in the presence of

photons, neutrinos, baryons, CDM and Λ,

$$H(z) = H_0 \left[\Omega_r^{(0)}(1+z)^4 + \Omega_m^{(0)}(1+z)^3 + \Omega_\Lambda^{(0)}\right]^{1/2}, \tag{2.41}$$

where we used Eq. (2.23) and the relation between the scale factor and the redshift, Eq. (2.24). Note also that $\Omega_m = \Omega_b + \Omega_c$ is the joint contribution from non-relativistic matter and, from the flatness condition, $\Omega_\Lambda = 1 - \Omega_r - \Omega_m$. The ΛCDM is the simplest model that fits the data, being quite successful on the job.

2.5 Cosmic distances

Cosmological distances are important observational tools in an expanding background. In non-static universe, measuring the physical distance to a given object is not trivial, and actually, there are several different definitions of distance. In order to compute them, we must retrieve information from other well-known properties of the object, such as redshift, observed luminosity or even observed characteristic angular size.

2.5.1 Comoving distance

The comoving distance remains unchanged in an expanding universe, in contrast to the physical distance, which scales proportionally to the scale factor. Hence we use it as the basic definition of distance. Light traveling radially along the χ direction satisfies the geodesic equation with $\mathrm{d}s^2 = -\mathrm{d}t^2 + a^2\mathrm{d}\chi^2 = 0$. Now, suppose a light beam was emitted at the time $t = t_1$ with $\chi = \chi_1(z)$, and the light reaches us at time $t = t_0$, with $\chi = 0$ (that is, $z = 0$). We define the comoving distance as

$$d_C \equiv \int_0^{\chi(z)} \mathrm{d}\chi = \int_{t(z)}^{t_0} \frac{c\,\mathrm{d}t'}{a(t')}.$$

Since $1 + z = 1/a$, we have $\mathrm{d}t = -\mathrm{d}z/[(1+z)H]$. Then, the comoving distance may be written as

$$d_C = \frac{1}{H_0}\int_0^z \frac{\mathrm{d}z'}{E(z')}. \tag{2.42}$$

2.5.2 Luminosity distance

The luminosity distance is related to the measurement of the flux from an object with known luminosity (standard candle), linking the luminosity to the expansion rate, and is used in supernovae observations. It is defined by

$$d_L^2 = \frac{L_s}{4\pi F}, \tag{2.43}$$

where F is the flux and L_s is the absolute luminosity of the source. Note that the observed luminosity L_0 (detected at $\chi = 0$ and $z = 0$) is different from L_s of the source (emitted at the comoving distance χ with redshift z). The flux F is defined by $F = L_0/S$, where $S = 4\pi\chi^2$ is the area of a sphere with comoving radius χ. Then, since the flux is conserved, the luminosity distance yields

$$d_L^2 = \chi^2 \frac{L_s}{L_0}. \tag{2.44}$$

Now we must find a relation between the luminosity at the source and the observed one. The absolute luminosity is defined by $L_s = \Delta E_1/\Delta t_1$, where ΔE_1 is the energy of light emitted in a given time-interval Δt_1. Similarly the observed luminosity is given by $L_0 = \Delta E_0/\Delta t_0$, where ΔE_0 is the energy of light detected at the time-interval Δt_0. Since the energy of a photon is inversely proportional to its wavelength we have that $\Delta E_1/\Delta E_0 = \lambda_0/\lambda_1 = 1 + z$, where we have used Eq. (2.24). Also, since $c = 1 = \lambda/\Delta t$ is constant, $\lambda_1/\Delta t_1 = \lambda_0/\Delta t_0$, which leads to $\Delta t_0/\Delta t_1 = \lambda_0/\lambda_1 = 1 + z$. Hence we find

$$\frac{L_s}{L_0} = \frac{\Delta E_1}{\Delta E_0}\frac{\Delta t_0}{\Delta t_1} = (1 + z)^2. \tag{2.45}$$

From Eqs. (2.44) and (2.45) the luminosity distance reduces to

$$d_L = (1 + z)\chi = (1 + z)d_C. \tag{2.46}$$

2.5.3 Angular diameter distance

The angular diameter distance is related to the size of the angle in the sky subtended by an object of known size (standard ruler). It is defined by

$$d_A \equiv \frac{l}{\theta}, \tag{2.47}$$

where l is the physical length, orthogonal to the line of sight and θ is the angle subtended in the sky. Since the source lies on the surface of a sphere with radius χ with the observer at the center, the angle may be written as

$$\theta = \frac{l/a}{\chi(a)},$$

therefore, the angular diameter distance takes the form

$$d_A = \frac{1}{1+z}\chi = \frac{1}{1+z}d_C. \tag{2.48}$$

Chapter 3

Dark energy

In this chapter, we first present the observational evidences for dark energy and how its properties can be probed using recent cosmological data. Later, we discuss the cosmological constant and its shortcomings, followed by an analysis of the alternatives to Λ: dark energy candidates with varying equation of state. Since the focus of the discussion is dark energy, from now on we often call the DE equation of state simply w, without any subscript, unless in cases there is room for confusion.

3.1 Observational evidence

The existence of dark energy is supported, and even required, by several cosmological observations, such as the age of the universe compared to oldest stars, supernovae observations, the anisotropies of the cosmic background radiation, baryon acoustic oscillations. For a comprehensive discussion on observational probes of dark energy, see Ref. [9]. In this section, we review some of this evidence. When discussing the CMB and BAO, concepts of cosmological perturbation theory are needed, but here we present only the bare minimum to understand the effect of DE on these phenomena. For a proper description of cosmological perturbations please check Refs. [3, 10].

3.1.1 The age of the universe

Even before the discovery of the accelerated expansion, it was known that a CDM-dominated universe could be younger than the oldest stars. In that context, the existence of dark energy could provide a solution, increasing the age of the cosmos.

Suppose that dark energy is described by a fluid with constant equation of state w so that its energy density can be written as

$$\rho_{de} = \rho_{de}^{(0)}(1+z)^{3(1+w)}.$$

In a universe filled with radiation, non-relativistic matter and dark energy, the Hubble parameter (normalized by H_0) (2.26) becomes

$$E(z) = \frac{H(z)}{H_0} = \left[\Omega_r^{(0)}(1+z)^4 + \Omega_m^{(0)}(1+z)^3 + \Omega_{de}^{(0)}(1+z)^{3(1+w)}\right]^{1/2}$$

and the cosmic age of the universe is

$$t_0 = \frac{1}{H_0}\int_0^\infty \frac{\mathrm{d}z}{(1+z)E(z)}. \tag{3.1}$$

The most important contributions to the integral Eq. (3.1) come from the low redshift terms, precisely when the energy density of radiation, $\Omega_r^{(0)} \sim 10^{-5}$, is negligible [see Eq. (2.37)]. Thus, the age of the spatially flat universe is given by

$$t_0 = \frac{H_0^{-1}}{3\sqrt{1-\Omega_m^{(0)}}} \ln\left(\frac{1+\sqrt{1-\Omega_m^{(0)}}}{1-\sqrt{1-\Omega_m^{(0)}}}\right),$$

where it was used $\Omega_m^{(0)} + \Omega_{de}^{(0)} = 1$ and we assumed, for simplicity's sake, that dark energy is the cosmological constant ($w = -1$). If we take the limit where there is no dark energy, i.e. $\Omega_{de}^{(0)} \to 0$, we have

$$t_0 = \frac{2}{3}H_0^{-1}. \tag{3.2}$$

From the local observations of the Hubble Space Telescope's Wide Field Camera 3 (WFC3) [11] the present Hubble parameter is constrained to be

$$H_0 = 73.24 \pm 1.74\,\mathrm{km\,s^{-1}\,Mpc^{-1}},$$

such that, the cosmic age of the universe according to Eq. (3.2) would be around $8.7\,\mathrm{Gyr} < t_0 < 9.1\,\mathrm{Gyr}$, which violates the stellar age bound: the age of globular clusters in the Milky Way are generally estimated to be larger than 11 Gyr [12–14]. Therefore, the lack of dark energy imposes serious issues on the flat universe.

3.1.2 Luminosity distance

The accelerated expansion of the universe was first reported independently by two research groups [15, 16] in the late 1990s. Both teams relied on observations of the luminosity distance of type Ia supernova (SNIa).

A supernova is a massive exploding star. It is classified in terms of the absorption lines in its spectra. Type II includes the spectral lines of hydrogen whilst type I does not. The latter can be further divided into three categories: type Ia, that includes the line of singly ionized silicon; type Ib, that includes a line of helium; and type Ic, that lacks the line of both silicon and helium [17].

We'll be interested in type Ia supernovae, which originates when a white dwarf in a binary system absorbs mass from its companion star until it reaches the Chandrasekhar limit and explodes, ejecting its mass and creating a shock wave that propagates away from the host galaxy [18].

The usefulness of SNIa relies on the fact that at peak brightness all events have roughly the same absolute magnitude. They are usually regarded as standard(izable) candles. The peak luminosities for different supernovae are not exactly the same and the spread is actually too large to be used as a cosmological probe. Fortunately, taking into account the shape of the light curve one can compute a standard observational value. The width of the light curve and the absolute magnitude are correlated in a way

that brighter supernovae have broader light curves. Therefore, measuring the apparent magnitude and the light curve, it is possible to infer the absolute magnitude.

The apparent magnitude is a measure of the brightness of a luminous object as seen by an observer on Earth. The relation between the apparent magnitude m and the apparent flux F of two given stellar objects is defined as

$$m_1 - m_2 = -2.5 \log_{10} \left(\frac{F_1}{F_2} \right). \tag{3.3}$$

The absolute magnitude of a light source is defined as the apparent magnitude the source would have if it were at a luminosity distance $d_L = 10\,\mathrm{pc}$. Since, according to Eq. (2.43), the observed flux is proportional to d_L^{-2}, Eq. (3.3) can be written as

$$m - M = 5 \log_{10} \left(\frac{d_L}{10\,\mathrm{pc}} \right).$$

The quantity $m - M$ is called distance modulus, and is represented by the Greek letter μ. Recasting the luminosity distance in Mpc one gets

$$\mu = 5 \log_{10} \left(\frac{d_L}{\mathrm{Mpc}} \right) + 25.$$

The luminosity distance Eq. (2.46) depends on the cosmology via an integral of the Hubble parameter,

$$d_L(z) = \frac{1+z}{H_0} \int_0^z \frac{\mathrm{d}z'}{E(z)},$$

hence, if we gather enough measurements of d_L we can estimate the cosmological parameters entering $H(z)$.

3.1.3 CMB

The existence of dark energy can also be probed using observations of temperature anisotropies in the cosmic microwave backgroud (CMB).

The CMB is the radiation remnant from the time of recombination, thus, according to the big bang cosmology, it is the oldest light we have access to. It was discovered

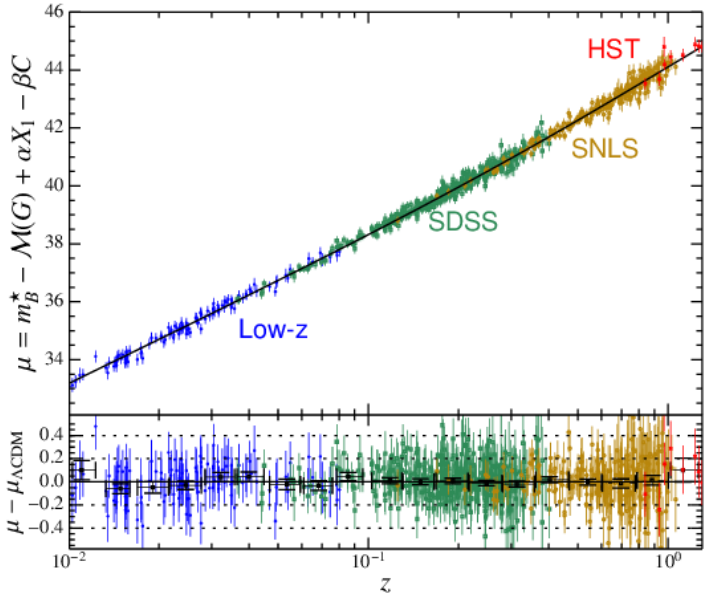

Figure 3.1: Distance modulus as function of the redshift $\mu(z)$ of the Joint Light-curve Analysis (JLA) combined sample and the baseline best-fit ΛCDM model. The bottom panel show the residues of the fitting. The distance modulus is sensitive to different cosmologies via the luminosity distance. From Ref. [19].

accidentally by radio astronomers A. Penzias and R. Wilson [20] in 1964, but its existence was speculated since the late 1940s in works by G. Gamow, R. Alpher, and R. Herman [21].

In the early universe, when it was about 300,000 years old and its temperature was above about 1 eV, the matter content consisted of a plasma of free electrons and nuclei (mostly protons). Photons were tightly coupled to electrons via Compton scattering, which in turn strongly interacted with protons via Coulomb scattering. Hence, the photons were trapped by the plasma, with mean free path much smaller than the Hubble horizon. The temperature was high enough so that any neutral hydrogen would by ionized [22].

Small perturbations, seeded by quantum fluctuations to this somewhat homogeneous plasma, oscillated acoustically, gravitational instability pulling in and the radiation pressure of the photons pushing out. As a result, the baryon-electron-photon fluid oscillated as sound waves, with velocity c_s^2.

As the universe expanded, both the plasma and the radiation filling it cooled down. The overall temperature became low enough so that nuclei and electrons combined to

form neutral atoms. After this epoch, called recombination, there was a deficit of free electron to interact with, hence the photons mean free path grew rapidly and became larger than the Hubble horizon. The photons decoupled, free streaming through the now transparent universe, and today they form the cosmic microwave background (redshifted by the cosmic expansion).

In addition to the redshift due to the expansion, the photons in the CMB are also gravitationally redshifted, causing the anisotropy of the observed spectrum. This property, called Sachs-Wolfe effect can be divided into two types [3]

The non-integrated Sachs-Wolfe effect is the primary source of anisotropy, caused by gravitational redshifts at, and prior to, the last-scattering surface. This is the main source of fluctuations, and its structure is mainly due to the acoustic oscillations and diffusion damping of the baryon-photon plasma before the decoupling epoch. The combination of these effects gives the microwave background its characteristic peak structure [see Fig. (3.2)].

The integrated Sachs-Wolfe (ISW) effect, on the other hand, is a result of the gravitational redshift that happened between the last-scattering surface and the observation of the spectra, hence it is not part of the primordial CMB. In a matter-dominated universe, the gravitational potential does not vary much, but if it is dominated by, say, dark energy, the potential does evolve, affecting the energy of the photons passing through it.

Thus, CMB observations are important to the study of dark energy in two aspects: DE can change the expansion history and hence the distance to the last scattering surface, with a shift in the acoustic peaks, and can cause the decay of gravitational potentials at late times, affecting the low-multipole anisotropies through the ISW effect.

The anisotropies of the CMB are characterized by fluctuations of its temperature

$$T(t, \mathbf{x}, \hat{p}) = \bar{T}(t)\,[1 + \Theta(t, \mathbf{x}, \hat{p})]$$

where $\bar{T}(t)$ is the smooth, isotropic, temperature field and $\Theta(t, \mathbf{x}, \hat{p})$ is the temperature

contrast,

$$\Theta(t, \mathbf{x}, \hat{p}) = \frac{\delta T(t, \mathbf{x}, \hat{p})}{T(t)}$$

that depends on the fluctuations $\delta T(t, \mathbf{x}, \hat{p})$. The perturbation field can be expanded in spherical harmonics [3]

$$\Theta(t, \mathbf{x}, \hat{p}) = \sum_{\ell=1}^{\infty} \sum_{m=-\ell}^{\ell} a_{\ell m}(t, \mathbf{x}) Y_{\ell m}(\hat{p}),$$

where the subscripts ℓ and m are conjugate to the real space unit vector $\hat{p}$, which gives the direction of propagation (momentum) of the incoming photons. The normalization condition for the spheric harmonics $Y_{\ell m}$ imposes

$$\int \mathrm{d}\Omega \, Y_{\ell m}(\hat{p}) Y^*_{\ell' m'}(\hat{p}) = \delta_{\ell \ell'} \delta_{m m'}.$$

The expansion coefficients are usually assumed to be statistically independent [17], which means that its mean value is zero ($\langle a_{\ell m} \rangle = 0$) and non-vanishing variance

$$C_\ell \equiv \left\langle |a_{\ell m}|^2 \right\rangle,$$

and, in terms of the temperature field $\Theta_\ell(k)$ in the Fourier space, the variance C_ℓ is given by [3]

$$C_\ell = \frac{2}{\pi} \int_0^\infty \mathrm{d}k \, k^2 |\Theta_\ell(k)|^2.$$

The C_ℓs give the power of each multipole ℓ, completely characterizing the cosmic microwave spectra. The precise shape of the spectrum depends both on the initial conditions (from inflation) and the cosmological parameters. In Fig. (3.2) we present the CMB power spectrum as measured by 2015 data release of the Planck satellite [4] and the corresponding best-fit ΛCDM prediction.

The angular size of the peaks is related do the multipole moments ℓ through

$$\theta = \frac{\pi}{\ell} \, [\mathrm{rad}] \tag{3.4}$$

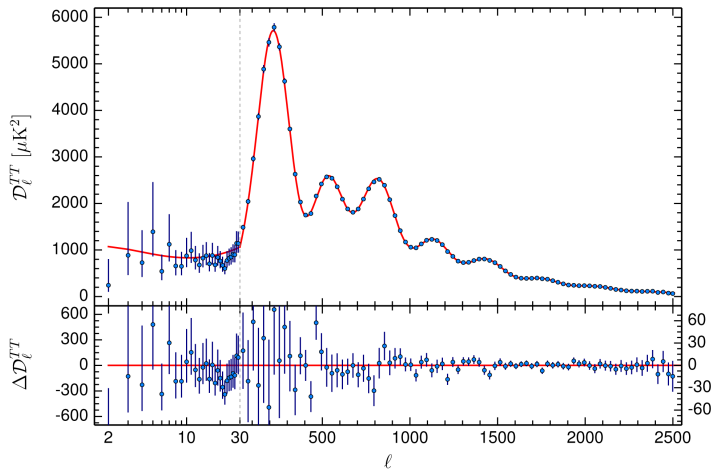

Figure 3.2: Planck 2015 temperature power spectrum as function of the multipoles ℓ. Here $\mathcal{D}_\ell \equiv \ell(\ell+1)C_\ell/2\pi$. The best-fit ΛCDM prediction is plotted in the upper panel and the corresponding residues in the lower panel. From [4].

which means that larger scales translate into smaller values of ℓ. In the spirit of Eq. (2.47), the characteristic angle for the location of the peaks can be defined as [17]

$$\theta_A = \frac{r_s(z_*)}{d_A^{(c)}(z_*)}, \tag{3.5}$$

where r_s is the sound horizon, the comoving angular diameter distance is

$$d_A^{(c)}(z) = (1+z)d_A(z),$$

where the physical (proper) d_A was defined in Eq. (2.48), and z_* is the redshift at the decoupling epoch. The sound horizon gives the distance covered by an acoustic wave in a given time interval. Hence a photon in the baryon-photon plasma travels

$$r_s(z_*) = \int_0^{\eta(z_*)} \mathrm{d}\eta\, c_s(\eta) = \int_{z_*}^{\infty} \frac{\mathrm{d}z}{H(z)} c_s(z), \tag{3.6}$$

until it decouples. The sound speed is given by $c_s = 1/\sqrt{3(1+R_s)}$ with the baryon-to-photon density ratio $R_s = 3\rho_b/4\rho_\gamma$, which evolves as

$$R_s = \frac{3\Omega_b^{(0)}}{4\Omega_\gamma^{(0)}} \frac{1}{1+z}.$$

The redshift at the decoupling epoch can be computed using Hu & Sugiyama's fitting formula [23]

$$z_* = 1048 \left[1 + 0.00124(\Omega_b^{(0)} h^2)^{-0.738}\right] \left[1 + g_1 (\Omega_m^{(0)} h^2)^{g_2}\right],$$

where

$$g_1 = \frac{0.0783(\Omega_b^{(0)} h^2)^{-0.238}}{1 + 39.5(\Omega_b^{(0)} h^2)^{-0.763}},$$
$$g_2 = \frac{0.560}{1 + 21.1(\Omega_b^{(0)} h^2)^{1.81}}.$$

The typical value for the redshift to the last-scattering surface is $z_* \approx 1100$.

The characteristic multipole ℓ corresponding to the angle (3.5) is

$$\ell_A = \frac{\pi}{\theta_A} = \pi \frac{d_A^{(c)}(z_*)}{r_s(z_*)}. \tag{3.7}$$

As discussed by Wang & Mukherjee [24], it is possible to summarize most information contained in the CMB power spectrum into just a few numbers. The fundamental principle is that using certain characteristic scales one can compress the CMB likelihood, making the process of parameter estimation much more efficient than the computationally expensive analysis of the full-spectrum likelihood, with little loss of information. The first of these quantities, as we can guess, is the characteristic multipole, define in Eq. (3.7). The other is the so-called CMB shift parameter

$$R = \sqrt{\Omega_m^{(0)} H_0^2}(1 + z_*) d_A(z_*). \tag{3.8}$$

The shift parameter R is a measure of the CMB temperature power spectrum along the line of sight, and different R will magnify or reduce the amplitude of the acoustic peaks. The angular scale of the sound horizon at last scattering, ℓ_A, characterizes the CMB temperature power spectrum in the transverse direction, with different l_A giving different distributions of peaks and trough [25, 26].

Usually, the baryon density $\Omega_b^{(0)}h^2$ is also included in the set of quantities that summarize the CMB data since it is required in making predictions for ℓ_A, thus correlated with it, and is a useful probe of late-time physics but not much sensitive to cosmological models [24].

The numbers ℓ_A, R and $\Omega_b^{(0)}h^2$, collectively called *distance priors*, provide an efficient and intuitive summary of CMB data, as far as dark energy constraints go, with one important caveat: the distance priors do not capture the information probed by the late-time ISW effect, hence its predictions are similar but not as robust as those derived using the full CMB spectrum [27].

3.1.4 BAO

Just as SNeIA are regarded as standard candles, i.e. objects whose distance can be inferred from its observed luminosity, baryon acoustic oscillations (BAO) provide a standard ruler: a characteristic size that can be used to compute distances. The BAO signal was first detected by the Sloan Digital Sky Survey back in 2005 [28], and is considered by some as "the standard ruler of choice for 21st-century cosmology" [29].

The physics behind the phenomena is quite well understood. Since baryons are tightly coupled to photons, via Compton drag, before the recombination epoch, the acoustic oscillations should also be imprinted in the baryon perturbations, thus should be observable in the distribution of galaxies.

To understand how the decoupling affects the galaxy distribution, consider, for now, the behavior of an overdensity at a particular initial location. Besides the baryon-electron-photon plasma, there is also dark matter in the universe. However, DM perturbations are only subject to gravitational instabilities, so it grows in place. Slightly after the decoupling, the baryonic part of the fluid is left in a spherical shell centered around the origin of the original overdensity, while the photons stream freely as CMB. The drag epoch is defined as the time at which the baryons were released from the Compton drag of the photons. The sound horizon at the drag epoch, i.e. the radius of the leftover shell, is the distance the sound waves could have propagated up until the

end of the Compton drag, hence it is given by Eq. (3.6) replacing the decoupling epoch z_* by the redshift at the drag epoch z_d. There is also a fitting formula for z_d, namely, Eisenstein & Hu's fitting formula [30]:

$$z_d = \frac{1291\,(\Omega_m^{(0)}h^2)^{0.251}}{1+0.659\,(\Omega_m^{(0)}h^2)^{0.828}}\left[1+b_1(\Omega_b^{(0)}h^2)^{b_2}\right],$$

where $\Omega_m^{(0)} = \Omega_b^{(0)} + \Omega_c^{(0)}$ is the matter density parameter and

$$b_1 = 0.313\,(\Omega_m^{(0)}h^2)^{-0.419}\left[1+0.607\,(\Omega_m^{(0)}h^2)^{0.674}\right],$$
$$b_2 = 0.238\,(\Omega_m^{(0)}h^2)^{0.233}.$$

The comoving size of the BAO scale is usually around 150 Mpc.

Both the dark matter at the center and the baryons on the shell seed gravitational instability, which grows to form galaxies at the origin and at the shell. Hence we expect current measurements to show an excess of pairs of galaxies separated by the acoustic scale. Of course, this happens around every perturbation, not only around one single overdensity. Therefore, to identify this feature, one measures the two-point correlation function of a patch of the sky.

The correlation function provides information about the angular and redshift distribution of galaxies, which can be summarized by [17]

$$\theta_s(z) = \frac{r_s(z_d)}{d_A^{(c)}(z)}, \tag{3.9}$$

$$\delta z_s(z) = r_s(z_d)H(z), \tag{3.10}$$

The angle $\theta_s(z)$ is analogous to the CMB acoustic peak angle (3.4) and corresponds to observations orthogonal to the line of sight. On the other hand, the quantity $\delta z_s(z)$ is related to the fluctuation along the line of sight.

Most of BAO surveys are not able to measure $\theta_s(z)$ and $\delta z_s(z)$ separately, but only

a spherically averaged combination

$$\left[\theta_s(z)^2 \delta z_s(z)\right]^{1/3} = \frac{r_s(z_d)}{\left[(1+z)^2 d_A^2(z)/H(z)\right]^{1/3}}$$

or the related effective distance [28]

$$D_V(z) = \left[(1+z)^2 d_A^2(z) \frac{z}{H(z)}\right]^{1/3}. \tag{3.11}$$

Note that D_V is a combination of an integral of $H(z)$ (through d_A) and a direct measurement of $H(z)$, so dark energy effects on the expansion might be probed using BAO measurements.

3.2 Cosmological constant

The simplest dark energy candidate is the so-called cosmological constant Λ, whose energy density is constant in time and space. The ΛCDM model is fully consistent with observations, explaining the current data with great success [4, 31]. The Lagrangian density for general relativity with a cosmological constant is rather simple, given by a linear term in the Ricci scalar R plus a constant Λ. Despite its appealing simplicity, it is remarkably difficult to explain why the energy scale required of the cosmological constant in order to account for the current accelerated expansion is much smaller than that predicted by particle physics for the vacuum energy. The vacuum energy density calculated using quantum field theory is many orders of magnitude greater than the observed energy density [32]. Another difficulty faced by Λ which must be accounted for is that its current energy density is surprisingly close to another independent quantity, namely, the matter energy density.

3.2.1 Einstein equations with a cosmological constant

The energy-momentum tensor on the R.H.S of Einstein's equations, Eq. (2.6), satisfies the conservation law $\nabla^\nu T_{\mu\nu} = 0$. Since, by the metric compatibility [2], the metric

tensor $g_{\mu\nu}$ satisfies the relation $\nabla^\nu g_{\mu\nu} = 0$, we are free to add the term $\Lambda g_{\mu\nu}$ to the Einstein equations:

$$R_{\mu\nu} - \frac{1}{2}Rg_{\mu\nu} + \Lambda g_{\mu\nu} = 8\pi G T_{\mu\nu}, \tag{3.12}$$

where Λ is the cosmological constant. Equation (3.12) is the most general local, coordinate-invariant, divergenceless, symmetric, two-index tensor we can construct solely from the metric and its first and second derivatives [33].

Einstein's equations in the presence of a cosmological constant can be derived from the principle of least action by adding to the Einstein-Hilbert action, Eq.(2.3), a constant term:

$$S = \frac{1}{16\pi G}\int \mathrm{d}^4x\,\sqrt{-g}(R - 2\Lambda) + S_m, \tag{3.13}$$

where, S_m is the action for matter and the multiplicative factor 2 is added for convenience. Extremizing Eq. (3.13) with respect to the metric, we find Eq. (3.12).

3.2.2 History of the cosmological constant

After the initial development of general relativity in 1915 [34], Albert Einstein attempted to apply his theory to the universe in 1917 [35]. By that time, he believed that the universe was static. However, from Eq.(2.16), it is clear that the scale factor a can vary over time (unless the universe is filled with a fluid with an equation of state precisely set to $w = 1/3$). Thus, he introduced the cosmological constant in order to meet his expectations. In a FLRW universe, Eq. (2.9), the Friedmann equations (3.12) become

$$H^2 = \frac{8\pi G}{3}\rho - \frac{K}{a^2} + \frac{\Lambda}{3}, \tag{3.14}$$

$$\frac{\ddot{a}}{a} = -\frac{4\pi G}{3}(\rho + 3p) + \frac{\Lambda}{3}. \tag{3.15}$$

Equation (3.15) indicates that Λ acts like a repulsive force, opposing gravity. These equations admit a static solution with positive spatial curvature and all parameters ρ, p, e Λ nonnegative, the so-called *Einstein's static solution*. Einstein's interest in

a static solution comes from the attempt to encompass to general relativity Mach's principle, which states that matter determines inertia. Moreover, such an assumption accounted for all the astronomical observations available at the time.

However, the static solution is unstable against perturbations to the energy density ρ. Any small deviation from the perfect equilibrium between the terms of Eq.(3.15) rapidly diverges from the static solution. With the discovery of Hubble's expansion of the universe [36], Λ was no longer necessary in explaining the observations.

3.2.3 The fine tuning problem

The current phase of cosmic acceleration can be explained, according to Eq.(3.14), setting the cosmological constant to be of the same order of the square of the Hubble parameter today, that is,

$$\Lambda \approx H_0^2 = (2.1332h \times 10^{-42}\,\mathrm{GeV})^2,$$

which is equivalent to an energy density

$$\rho_\Lambda \approx \frac{\Lambda m_{pl}^2}{8\pi} \approx 10^{-47}\,\mathrm{GeV}^4 \approx 10^{-123} m_{pl}^4, \tag{3.16}$$

where $m_{pl} = 1/\sqrt{G} \approx 10^{19}\,\mathrm{GeV}$ is the Planck mass and we set $h = 0.7$.

The natural explanation to the energy density (3.16) is the vacuum energy of empty space, $\langle\rho\rangle$. The zero-point energy of a quantum field of mass m, momentum k, and frequency ω is given by

$$E = \frac{\omega}{2} = \frac{\sqrt{k^2+m^2}}{2},$$

assuming $\hbar = c = 1$. The vacuum energy density is given by the integral of the zero-point energies up to a cut-off scale k_{max} that specifies the limits of applicability of the theory at hand:

$$\rho_{vac} = \int_0^{k_{max}} \frac{\mathrm{d}^3k}{(2\pi)^3}\frac{1}{2}\sqrt{k^2+m^2}.$$

Since the integral is dominated by large-k modes, we find

$$\rho_{vac} = \int_0^{k_{max}} \mathrm{d}k \, \frac{4\pi k^2}{(2\pi)^3} \frac{1}{2} \sqrt{k^2 + m^2} \approx \frac{k_{max}^4}{16\pi^2}.$$

General relativity is expected to be valid up to the Planck scale, so assuming that the cut-off is m_{pl}, the vacuum energy density would be something like

$$\rho_{vac} \approx 10^{74}\,\mathrm{GeV}^4,$$

which is roughly 10^{121} times larger than the observed value (3.16). It is important to point out that, even adopting other, more conservative, typical values appearing in particle physics for the cut-off scale, the discrepancy does not go away. For instance, the QCD scale $k_{max} \approx 0.1\,\mathrm{GeV}$ yields $\rho_{vac} \approx 10^{-3}\,\mathrm{GeV}^4$, still much larger than (3.16).

The vanishing of a constant usually signal the existence of some symmetry, however, there isn't any known symmetry which could enforce a vanishing vacuum energy without challenging other aspects of particle physics theory.

3.2.4 The coincidence problem

Another problem that all dark energy candidates, and not just the cosmological constant, must face is that the current value of its energy density is practically equal to another number which, at first, evolves completely different: the current matter energy density. Throughout much of the universe's history these two numbers had very distinct values such that $\Omega_\Lambda^{(0)}$ is doubly unlikely since, in addition to being very small when compared to all other fundamental energy scales, it is of the same order of $\Omega_m^{(0)}$.

Contrary to the fine tuning problem, which has an observational origin, the coincidence problem depends on the model chosen to explain DE. Assuming that it is not merely a coincidence, there are several proposals to explain the puzzle: tracker-type models, where the energy density ρ_{de} responds to the behavior of ρ_m, so that for several initial conditions ρ_{de} tracks the matter energy density; scaling models, in which the equation of state of dark energy and of dark matter are related, causing the ratio

$r = \rho_m/\rho_{de}$ to be constant for a long time; or even interacting models, in which it is assumed that there is an interaction between dark energy and a matter component, say, dark matter, and thus $\Omega_{de}^{(0)}$ and $\Omega_c^{(0)}$ are of the same order because there is a dynamic exchange of energy in the dark sector along the evolution of the universe.

Although there are several attempts, the coincidence problem is far from being solved, and probably will only be resolved when the nature of dark energy is fully understood. A successful model for DE must be able to explain it away. Meanwhile, it is useful to take both the coincidence and the fine tuning problems as a guide pointing towards theoretical directions to elucidate the accelerated expansion.

3.3 Alternatives to Λ

Even though the cosmological constant Λ describes remarkably well the current data, it has its shortcomings, as we just saw, which lead us to consider alternatives to address the current expansion phase.

As a first guess, one could relax the requirement $w = -1$ and let the equation of state be another cosmological parameter whose value must be constrained observationally. Assuming that dark energy is described by a fluid with constant equation of state w, its energy density would be given by

$$\rho_{de}(z) = \rho_{de}^{(0)}(1+z)^{3(1+w)}. \tag{3.17}$$

This simple extension of the ΛCDM paradigm is usually called wCDM, for obvious reasons.

Despite the fact that observations constraint the current value of w to be close to -1, it says very little about its value in the past. Therefore, we are enticed to consider models where w varies dynamically with time. Phenomenologically, it is usual to consider some time-dependent parametrization as, for instance, a Taylor expansion

$$w(z) = \sum_{n=0} w_n f_n(z),$$

where the coefficients w_n should be fixed by observations and $f_n(z)$ are functions of the redshift. Several 2-parameter extensions have been proposed in the literature, among which we highlight:

- Linear redshift parametrization [37–39]:

$$w(z) = w_0 + w_1 z.$$

- Chevallier–Polarski–Linder (CPL) [40, 41]:

$$w(z) = w_0 + w_1 \frac{z}{1+z}.$$

- Jassal-Bagla-Padmanabhan (JPB) [42]

$$w(z) = w_0 + w_1 \frac{z}{(1+z)^2}.$$

- Barboza-Alcaniz (BA) [43]

$$w(z) = w_0 + w_1 \frac{z(1+z)}{1+z^2}.$$

All these possibilities fit well the observations in the low-redshift region. Nevertheless, being phenomenological approximations, they usually face challenges explaining the entire expansion history of the universe. For instance, the linear redshift parametrization has problems at high redshift, whereas CPL and JPB are not well defined in the future [43]. The BA parametrization was put forward as a tentative fix to this limitations. Anyhow, for each of these proposals, the energy density is given by

$$\rho_{de} = \rho_{de}^{(0)} \exp\left\{ \int \frac{\mathrm{d}z}{1+z} 3\left[1 + w(z)\right] \right\}$$

where the integral must be computed accordingly.

3.4 Dark energy as a scalar field

In addition to parametrized models, scalar fields are also good dark energy candidates since it is the simplest field that can lead to a dynamical equation of state.

Here we will develop a general formalism that can be applied to scalar fields minimally coupled to Einstein's gravity. This approach is quite versatile since it allows the description of a range of scalar field models in the same framework. Although it was developed in the context of K-inflation, it is also useful in the study of dark energy.

Consider the most general action for a minimally coupled scalar field, which involves at most the first derivatives of the field

$$S = \int \mathrm{d}^4x \sqrt{-g} \left[\frac{1}{2\kappa^2} R + p(\phi, X) \right], \tag{3.18}$$

where $\kappa^2 = 8\pi G$, the Lagrangian density $p(\phi, X)$ is a function of the field ϕ and the kinetic term

$$X = -\frac{1}{2} g^{\mu\nu} \partial_\mu \phi \partial_\nu \phi.$$

We called the Lagrangian density p instead of the usual notation $\mathcal{L}$ because, as we will see, it plays the role of pressure [44]. Also, as customary in the field theory literature, we'll omit the *density* and just call it *the Lagrangian*. Varying the action with respect to the field, we find the equation of motion [45]

$$G^{\mu\nu} \nabla_\mu \nabla_\nu \phi + 2X \frac{\partial^2 p}{\partial X \partial \phi} - \frac{\partial p}{\partial \phi} = 0, \tag{3.19}$$

where

$$G^{\mu\nu} = \frac{\partial p}{\partial X} g^{\mu\nu} + \frac{\partial^2 p}{\partial X^2} \nabla^\mu \phi \nabla^\nu \phi.$$

Note that here $G^{\mu\nu}$ is not the Einstein tensor. Now, using Eq. (2.7), the energy-momentum tensor associated to this action reads

$$T_{\mu\nu} = \frac{\partial p}{\partial X} \partial_\mu \phi \partial_\nu \phi + p g_{\mu\nu}. \tag{3.20}$$

In order to fulfill the homogeneity and isotropy requirements of the FLRW universe, Eq. (3.20) takes the form of a perfect fluid, Eq. (2.12), with velocity $u_\mu = \partial_\mu\phi/\sqrt{2X}$ and

$$\rho_\phi = 2Xp_{,X} - p \tag{3.21}$$

$$p_\phi = p. \tag{3.22}$$

Here $p_{,X}$ stands for the derivative of p with respect to X. The equation of state, Eq. (2.17), reads

$$w_\phi = \frac{p_\phi}{\rho_\phi} = \frac{p}{2Xp_{,X} - p}, \tag{3.23}$$

so, with a suitable choice of p the scalar field can have an equation of state that describes dark energy. As long as the condition $|2Xp_{,X}| \ll |p|$ is met, w_ϕ can be close to -1. Now, taking into account that

$$\dot{\rho_\phi} = \frac{\partial\rho_\phi}{\partial X}\dot{X} + \frac{\partial\rho_\phi}{\partial\phi}\dot{\phi},$$

and using Eq. (2.15), we find the following expression for the time derivative of the pressure

$$\begin{aligned}\dot{p}_\phi &= \frac{\partial p_\phi}{\partial X}\dot{X} + \frac{\partial p_\phi}{\partial\phi}\dot{\phi} \\ &= -3c_s^2H(\rho_\phi + p_\phi) + \dot{\phi}\left(\frac{\partial p_\phi}{\partial\phi} - c_s^2\frac{\partial\rho_\phi}{\partial\phi}\right),\end{aligned}$$

where we introduced the quantity

$$c_s^2 = \frac{p_{\phi,X}}{\rho_{\phi,X}} = \frac{p_{\phi,X}}{p_{\phi,X} + 2Xp_{\phi,XX}}, \tag{3.24}$$

which plays the role of the sound speed for perturbations in the density field [46]. So, if the kinetic term in the Lagrangian for the scalar field is not linear in X, the sound speed of the fluctuations will differ from unity.

To illustrate the formalism, we shall apply it to specific scalar field models.

Quintessence

Quintessence is described by an ordinary scalar field minimally coupled to gravity, with canonical kinetic energy and whose potential can lead to late time acceleration [47,48]. It is the simplest field since it lacks internal degrees of freedom, do not introduce preferred directions, is typically weakly clustered, and can easily drive an inflationary period [45]. The Lagrangian for quintessence is given by

$$p(\phi, X) = X - V(\phi), \tag{3.25}$$

where $V(\phi)$ is the potential of the field. In a flat FLRW background, the energy and pressure densities are

$$\rho_\phi = \frac{1}{2}\dot{\phi} + V(\phi), \tag{3.26}$$

$$p_\phi = \frac{1}{2}\dot{\phi} - V(\phi), \tag{3.27}$$

and the equation of state is

$$w_\phi = \frac{p_\phi}{\rho_\phi} = \frac{\dot{\phi} - 2V(\phi)}{\dot{\phi} + 2V(\phi)}. \tag{3.28}$$

Note that since p is linear in X, the sound speed, Eq. (3.24), is equal to 1. This means that we do not expect clustering. The dynamics of quintessence is given by the continuity equation, Eq. (2.15), using the above definition of ρ_ϕ and p_ϕ, or directly from Eq. (3.19),

$$\ddot{\phi} + 3H\dot{\phi} + \frac{\mathrm{d}V}{\mathrm{d}\phi} = 0. \tag{3.29}$$

In a scalar field dominated universe, the acceleration equation, Eq. (2.16), reads

$$\frac{\ddot{a}}{a} = -\frac{\kappa^2}{3}\left[\dot{\phi}^2 - V(\phi)\right],$$

thus, we find that accelerated expansion takes place if $\dot{\phi}^2 < V(\phi)$, that is if the potential is flat, shallow enough for the field to evolve slowly along it.

From Eq. (3.28) we see that w_ϕ smoothly interpolates between -1 and 1. In this case the integrated form of the continuity equation, Eq. (2.20),

$$\rho_\phi = \rho_\phi^{(0)} \exp\left[-\int \frac{\mathrm{d}a}{a} 3(1+w_\phi)\right]$$

tells us that in the slow-roll limit, $\dot{\phi}^2 \ll V(\phi)$, since $w_\phi = -1$ the energy density is constant $\rho = \text{const.}$ and the field acts like a cosmological constant. Conversely, if $\dot{\phi}^2 \gg V(\phi)$, we would have $w_\phi = 1$ and the energy density would evolve as $\rho \propto a^{-6}$, characterizing a stiff matter. In other cases, it is piecewise interpolated by

$$\rho_\phi \propto a^{-m}, \qquad 0 < m < 6.$$

Unlike the cosmological constant, the energy density of quintessence does not have to be negligible when compared to radiation or matter in the early universe, and the existence of the so-called tracker solutions helps to alleviate the coincidence problem. Usually, one requires that ρ_ϕ tracks the energy density of the dominant component (matter or radiation) so that the dark energy density emerges at late times as the dominant component [49, 50].

Many quintessence potentials have been proposed throughout the years, both on phenomenological (leading to attractive cosmological properties) and theoretical (from extensions of the standard model of particle physics) grounds. Roughly speaking, it can be divided into "freezing" models and "thawing" models [17, 51]. In freezing models, the field was rolling along the potential in the past but it slows down when the universe enters the current accelerated phase. These are essentially tracking models [52]. Some examples of this class are

$$V(\phi) = M^{4+n}\phi^{-n}, \quad (n > 0),$$
$$V(\phi) = M^{4+n}\phi^{-n}\, \exp\!\left(\alpha\phi^2/m_{Pl}^2\right),$$

where M is a mass scale, and $m_{Pl}^2 = G^{-1}$ is the Planck mass. On the other hand, in

thawing models, the field was frozen by Hubble friction (the $H\dot{\phi}$ term in (3.29)) until recently, when it started to roll down to the minimum. In the past, $w_\phi \approx -1$, but becomes less negative with time. Potentials with these characteristics are

$$V(\phi) = V_0 + M^{4-n}\phi^n, \quad (n > 0),$$
$$V(\phi) = M^4 \cos^2(\phi/f),$$

where f is a global spontaneous symmetry breaking scale [53].

For its robustness and simplicity, quintessence models are the prototypical scalar field dark energy models and have been widely explored in the literature [52, 54–56].

Tachyon field

The tachyon field was first introduced in the context of string field theory as an attempt to understand the tachyonic mode present in the spectrum of the string, characterized by a negative mass-squared state [57]. The nonlinear Lagrangian is given by [58]

$$p(\phi, X) = -V(\phi)\sqrt{1 - 2X}. \tag{3.30}$$

In a flat FLRW background, the energy density and pressure are

$$\rho_\phi = \frac{V(\phi)}{\sqrt{1 - \dot{\phi}^2}}, \tag{3.31}$$
$$p_\phi = -V(\phi)\sqrt{1 - \dot{\phi}^2}, \tag{3.32}$$

and the equation of state is

$$w_\phi = \frac{p_\phi}{\rho_\phi} = \dot{\phi}^2 - 1. \tag{3.33}$$

Since the derivative of the field is constrained by the Lagrangian to be $\dot{\phi}^2 < 1$, the equation of state is bounded by $-1 < w_\phi < 0$. Another interesting feature of the tachyon field is that the speed of sound is not equal to unity, like for the canonical

scalar field. Actually, from Eq. (3.24),

$$c_s^2 = 1 - \dot{\phi}^2 = -w_\phi. \tag{3.34}$$

Finally, from Eq. (3.19), we find the equation of motion

$$\frac{\ddot{\phi}}{1-\dot{\phi}^2} + 3H\phi + \frac{1}{V}\frac{\mathrm{d}V}{\mathrm{d}\phi} = 0. \tag{3.35}$$

When $\dot{\phi}$ is small (compared to unity), we have $w_\phi \to -1$, and the field acts like a cosmological constant, whereas when $\dot{\phi} \approx 1$ it behaves like pressureless dust, $w_\phi = 0$. In general, the energy density evolves as

$$\rho_\phi \propto a^{-m}, \quad 0 < m < 3.$$

As in quintessence models, the field relies on its potential energy to sustain the late-time inflationary phase. In Chapter (4) we discuss further aspects of the tachyon field.

K-essence

Both quintessence and tachyon fields rely on the slowly varying potential to explain the current expansion phase of the universe. Nevertheless, such phenomena might be realized by modifications to the kinetic energy of ϕ. Scalar fields with non-canonical kinetic dependence are often found in particle physics, and one might ask if they can play a role in dark energy scenarios.

These fields were first introduced in the cosmological context to explain inflation at high energies in a model called K-inflation [44, 46]. Later, this scenario was applied to dark energy [59] and called K-essence [60].

As already mentioned, the main feature of K-essence is that the cosmic acceleration can be realized by the kinetic term X. The field only behaves as a negative pressure component after the matter-radiation equality, dominating the energetic budget of the

universe after the matter epoch [60].

As with quintessence, K-essence fields also exhibits tracking solutions, with attractors in the space of solutions during both radiation and matter-dominated epochs.

Some examples of K-essence fields are: low-energy effective string theory with derivative terms of higher-order than X [61], dilatonic ghost condensate [62,63], Dirac-Born-Infeld (DBI) theories [64, 65], among others [66–68]. Despite the fact that the tachyon field relies on its potential energy to lead to the late-time inflation, some authors classify it as a K-essence field simply because of the form of its Lagrangian [17].

3.4.1 Challenges for scaling cosmologies

One way to solve, or at least to alleviate, the coincidence problem is by means of the so-called *scaling solutions* [49, 69], in which the ratio

$$r = \frac{\rho_c}{\rho_\phi}, \tag{3.36}$$

with $r > 0$, remains constant for a certain period, explaining why the CDM energy density ρ_c and ρ_ϕ are currently of the same order. If the solution is an attractor, so that for different initial conditions the field sooner or later enters the scaling regime, the coincidence problem is taken care of.

In order to be successful, scaling models must be able to reproduce the well-known history of the universe, with an epoch dominated by radiation (soon after inflation), followed by a matter-dominated era (long enough to allow structure formation), and finally a period of accelerated expansion fueled by dark energy.

The current expansion can be explained in two different scenarios. In the first, the field eventually leaves the scaling regime characterized by Eq.(3.36), moving to an accelerated state. Such an effect can be achieved if the slope of the potential becomes shallower in low redshifts when compared with the potential at the time of the scaling [70, 71]. However, the mechanism to exit scaling regime creates a new coincidence problem [72]. In the second scenario, late-time inflation is actually realized

at the attractor fixed point, that is, the system tends asymptotically to an accelerated scaling solution.

Both canonical and tachyon scalar fields admit scaling attractors, but the equation of state for dark matter should be negative in order to realize the accelerated expansion, making such solution physically unacceptable [49,73,74]. One way around this problem is to assume that there is a coupling between DM and DE. In this case, the scaling solution would become feasible, provided the coupling is relatively large [75]. However, it was later shown the impossibility of cosmological solutions that reproduce the matter era followed by the dark energy domain with a constant DM-DE ratio for a large class of scalar field models [76]. Although there are still attempts to solve the coincidence problem by means of scaling cosmologies, such efforts must face great challenges.

3.5 Interacting dark energy

In addition to gravity, dark energy candidates may also experience a new fifth force. That is the case of Interacting Dark Energy (IDE) models where we consider the possibility that dark energy, seen as a scalar field or dynamic fluid, can interact with other components of the universe. The interaction couples the evolution of species that in a standard ΛCDM universe would evolve independently. The individual energy-momentum tensor of the interacting species, in general, is not separately conserved. Only the total $T^{\mu\nu}$ is.

One might consider coupling DE to baryons, neutrinos, dark matter, or even a universal coupling to all the matter components. The coupling between the scalar field and baryons can be investigated through its effects on local (solar system) measurements, on tests of the equivalence principle, or on the variation of fundamental constants over cosmological time scales. Such interaction should be very small and it is not expected to have large cosmological implications [77,78]. There is also the possibility of interaction between dark energy and neutrinos as in the models of *Mass-Varying Neutrinos* (MaVaNs) [79,80], and *growing neutrinos* [81].

Arguably, the most interesting case is the interaction between dark energy and dark

matter. Since DE and DM dominate the current energy budget of the universe, and its fundamental nature is not known for certain, it is reasonable to consider such interaction. Furthermore, the coupling might explain why their energy densities are of the same order, solving (or at least alleviating) the coincidence problem. This possibility has been widely explored for some time now, considering several dark energy candidates such as: quintessence [82–84], tachyon scalar fields [85], fluids with constant equation of state [86–88] and holographic models [89–91]. A recent and fairly comprehensive review of the theoretical and observational aspects and future prospects of interacting DE/DM models can be found in [72].

Finally, when a universal coupling is present the interaction can be explicitly reformulated into a non-minimal coupling to gravity, after a redefinition of the metric and matter fields (Weyl scaling), resulting in a scalar-tensor theory of modified gravity in the presence of uncoupled matter fields [63].

Usually, the coupling can be introduced at the Lagrangian level by making the mass M of the matter field dependent on the scalar field ϕ, defining a function $M(\phi)$ that specifies the type of interaction,

$$S = \int \mathrm{d}^4x \sqrt{-g} \left[p(\phi, X) + \mathcal{L}_{kin}[\psi] - M(\phi)\bar{\psi}\psi \right],$$

where $\mathcal{L}_{kin}[\psi]$ is the kinetic part of the Lagrangian for the matter field ψ. Similarly, the coupling between ϕ and a generic matter component, that we will indicate by the α index, can be treated as an external source $Q_{(\alpha)\mu}$ in Bianchi identities:

$$\nabla_\nu T^\nu_{(\alpha)\mu} = Q_{(\alpha)\mu}, \tag{3.37}$$

with the constraint

$$\sum_\alpha Q_{(\alpha)\mu} = 0.$$

The background continuity equation is given by the zero component of Eq. (3.37),

$$\dot{\rho}_\phi + 3H(1+w_\phi)\rho_\phi = -Q = -\beta(\phi)(1-3w_\alpha)\rho_\alpha\dot{\phi}, \tag{3.38}$$

$$\dot{\rho}_\alpha + 3H(1+w_\alpha)\rho_\alpha = +Q = \beta(\phi)(1-3w_\alpha)\rho_\alpha\dot{\phi}, \tag{3.39}$$

for the scalar field ϕ coupled to a single fluid α by the function $\beta(\phi)$, which in general may not be constant. The mass $M(\phi)$ and coupling $\beta(\phi)$ functions are related by [92]

$$Q_{(\phi)\mu} = \frac{\partial \ln M(\phi)}{\partial\phi} T_\alpha \partial_\mu\phi, \quad M(\phi) = \bar{M}e^{-\beta(\phi)\phi}. \tag{3.40}$$

The dark energy evolution depends on the trace T_α of the energy-momentum tensor, and consequently, the energy density and pressure of the species α.

Another possible approach is to consider a phenomenological interaction. Instead of identifying $Q_{(\alpha)\mu}$ with the matter-field mass term in the Lagrangian, we start from Eq. (3.37) by identifying DE as a fluid, and then we parameterize the interaction as a function of the energy densities of the coupled components and of a time scale (usually, the Hubble parameter) [86, 87, 90, 93]. The Taylor expansion up to first order of the zero component would be

$$Q_{(\alpha)} = 3H(\xi_1\rho_{de} + \xi_2\rho_\alpha), \tag{3.41}$$

where the coefficients ξ_1 and ξ_2 are coupling constants that must be determined observationally [94, 95]. As an example, consider a cosmological model with an interaction between dark matter and dark energy. The conservation equations read

$$\dot{\rho}_{de} + 3H\left(1+w\right)\rho_{de} = Q_{de} = -Q, \tag{3.42}$$

$$\dot{\rho}_c + 3H\rho_c = Q_c = +Q. \tag{3.43}$$

and according to Eq. (3.41), the coupling is given by $Q = 3H(\xi_1\rho_{de} + \xi_2\rho_c)$. The stability of this model for a constant dark energy equation of state w was studied in [96]. It was found that the curvature perturbation is stable when the interaction is proportional to the energy density of dark energy, i.e., when $\xi_1 \neq 0$ and $\xi_2 = 0$, in the

range $w < 0$ except for the divergence at the phantom crossing line ($w = -1$). Here we call this model IDE1. For the interaction proportional to the dark matter energy density, $\xi_1 = 0$ with $\xi_2 \neq 0$, the curvature perturbation is only stable in the phantom region, when w is smaller than -1. This possibility will be referred to as IDE2.

After the specification of the coupling, Eqs. (3.42) and (3.43) can be integrated. For IDE1, the energy densities for dark energy and dark matter are given by [97]

$$\begin{aligned}\rho_{de}(z) &= \rho_{de}^{(0)}(1+z)^{3(1+w+\xi_1)},\\ \rho_c(z) &= \rho_c^{(0)}(1+z)^3 + \rho_{de}^{(0)}\frac{\xi_1}{\xi_1+w}\left[(1+z)^3 - (1+z)^{3(1+w+\xi_1)}\right]\end{aligned}$$

whereas, for IDE2,

$$\begin{aligned}\rho_{de}(z) &= \rho_{de}^{(0)}(1+z)^{3(1+w)} + \rho_c^{(0)}\frac{\xi_2}{\xi_2+w}\left[(1+z)^{3(1+w)} - (1+z)^{3(1-\xi_2)}\right],\\ \rho_c(z) &= \rho_c^{(0)}(1+z)^{3(1-\xi_2)}.\end{aligned}$$

Thus, in a cosmological setting with only dark matter and dark energy, the expansion history would be given by

$$H(z) = H_0\left[\Omega_c^{(0)} f_c(z) + \Omega_{de}^{(0)} f_{de}(z)\right]^{1/2}, \tag{3.44}$$

where the functions $f_c(z)$ and $f_{de}(z)$ carry the information about the evolution of dark matter and dark energy, respectively:

$$\begin{aligned}f_c(z) &= (1+z)^3,\\ f_{de}(z) &= \frac{\xi_1}{\xi_1+w}(1+z)^3 + \left(1 - \frac{\xi_1}{\xi_1+w}\right)(1+z)^{3(1+w+\xi_1)},\end{aligned}$$

for IDE1, and

$$\begin{aligned}f_c(z) &= \frac{\xi_2}{\xi_2+w}(1+z)^{3(1+w)} + \left(1 - \frac{\xi_2}{\xi_2+w}\right)(1+z)^{3(1-\xi_2)},\\ f_{de}(z) &= (1+z)^{3(1+w)},\end{aligned}$$

for IDE2.

Chapter 4

Tachyon scalar field

In this chapter, we explore some of the features of the tachyon scalar field and present the interacting tachyon model that will be compared to observations in the next chapter.

The tachyon is an unstable field which has become important in string theory through its role in the Dirac-Born-Infeld (DBI) action which is used to describe the D-brane action [58, 98]. It was first proposed in the late 1990s by Ashoke Sen [99, 100] as an attempt to understand the negative mass-squared mode present in string theory [57, 101]. Sen showed that the decay of D-branes produces a pressureless gas that resembles classical dust [102, 103]. In cosmological settings, it can act as a source of dark matter and can lead to a period of inflation depending on the form of the associated potential and on the initial conditions [104–106]. For a class of potentials, it can be regarded as the source of dark energy [74, 107–110].

Although the effective Lagrangian (3.30) was originally derived from string field theory, it may have another physical interpretation [107]. The Lagrangian density for the canonical scalar field Eq. (3.25) can be seen as the generalization of the classical, non-relativistic particle's Lagrangian [1]

$$L = \frac{1}{2}m\dot{q}^2 - V(q) \Rightarrow \mathcal{L} = -\frac{1}{2}\partial_\mu\phi\partial^\mu\phi - V(\phi)$$

[1] In this brief discussion, we will use the conventional field theory notation and will refer to the Lagrangian density by the letter $\mathcal{L}$.

where the particle's (one-dimensional) position $q(t)$ has been promoted to a extended field configuration $\phi(\mathbf{x})$.

By the same token, if we consider a relativistic particle whose Lagrangian is given by

$$L = -m\sqrt{1-\dot{q}^2}, \tag{4.1}$$

we note that the Lagrangian density Eq. (3.30) can be seen as the generalization of Eq. (4.1) when we promote the coordinate to a field configuration and let the mass become a function of the field itself:

$$L = -m\sqrt{1-\dot{q}^2} \Rightarrow \mathcal{L} = -V(\phi)\sqrt{1+\partial_\mu\phi\partial^\mu\phi}$$

Hence, quintessence is related to the non-relativistic particle the same way as the tachyons are related to relativistic ones.

It has been argued [105], that another motivation to study the tachyon scalar field arises from the fact that if, at dawn of quantum field theory, one had proceeded from non-relativistic classical mechanics to relativistic classical mechanics and upgraded q to a field, instead of starting from non-relativistic classical mechanics to non-relativistic quantum mechanics (Schrodinger's equation) and then trying put it in a relativistic formulation, one would have naturally found the Lagrangian Eq. (3.30).

4.1 Cosmology with tachyon field

4.1.1 Tachyon as a unified DE/DM candidate

To explore the cosmological properties of the tachyon scalar field, we wrote the action that minimally couples it to gravity and found that the energy and pressure densities,

in a flat FLRW universe, are given by Eqs. (3.31) and (3.32),

$$\rho_\phi = \frac{V(\phi)}{\sqrt{1-\dot{\phi}^2}}, \tag{4.2}$$

$$p_\phi = -V(\phi)\sqrt{1-\dot{\phi}^2}. \tag{4.3}$$

An interesting characteristic of this model is that ρ_ϕ and p_ϕ can be split into two contributions [105]

$$\rho_\phi = \rho_{de} + \rho_{dm},$$

$$p_\phi = p_{de} + p_{dm},$$

where we conveniently defined

$$\rho_{dm} = -\frac{V(\phi)\partial_\mu\phi\partial^\mu\phi}{\sqrt{1+\partial_\nu\phi\partial^\nu\phi}}, \qquad p_{dm} = 0,$$

$$\rho_{de} = V(\phi)\sqrt{1+\partial_\nu\phi\partial^\nu\phi}, \qquad p_{de} = -\rho_{de}.$$

In this setting, the pressureless "dm" component acts like dust, with a vanishing equation of state, thus it would be a dark matter candidate, whereas the "de" contribution has negative pressure, with $w_{de} = -1$, and it would be a natural candidate to dark energy. In fact, if we were able to find a field configuration whose net effect in the past is matter-like, evolving towards the present accelerated state, we would be able to explain the whole dark sector with a single field. Conversely, as far as cosmological observations go, it would be possible to replace the tachyon field by two interacting fluids [111]. Before exploring unified tachyonic models, it might be elucidating to take a look at a related class with similar properties: the Chaplygin gas.

Unified Dark Matter (UDM) models, also known as *quartessence* [112], are attempts to describe both dark matter and dark energy using one single fluid or scalar field. One of the first proposed models was the Chaplygin gas [113], which consists of a fluid

described by the equation of state

$$p = -\frac{A}{\rho}$$

where A is a positive constant. A natural extension is the so-called generalized Chaplygin gas (GCG) [114], where

$$p = -\frac{A}{\rho^{\alpha}}. \tag{4.4}$$

If $\alpha > 0$, the pressure is suppressed in the past (when the energy density is large), but it gains importance as time goes by, becoming more negative. Thus, the fluid initially behaves like pressureless dust and like dark energy in the recent universe. In fact, by substituting Eq. (4.4) into the continuity equation, Eq. (2.15), we find

$$\rho(a) = \left[A + Ba^{-3(1+\alpha)}\right]^{1/(1+\alpha)} \tag{4.5}$$

where B is an integration constant. Clearly, $\rho \propto a^{-3}$ in early times and $\rho =$ constant in the late epoch.

Despite being able to describe quite well the expansion history of the universe, GCG models are under great pressure from both structure formation and cosmic microwave background anisotropy observations [115, 116]. In the perturbative regime [117, 118], when GCG predictions for the matter power spectrum were compared with observations [119], the parameter α was constrained to be $|\alpha| < 10^{-5}$, whereas when compared to CMB anisotropy [115, 120, 121] the result was $0 \leq \alpha < 0.2$. Such constraints make the GCG model virtually indistinguishable from standard ΛCDM ($\alpha = 0$), and completely rule out the original Chaplygin gas ($\alpha = 1$).

Note that the Chaplygin gas can be seen as a particular case of the tachyonic scalar field with a constant potential $V_0 = \sqrt{A}$ [122, 123]. Indeed, for a constant potential we can solve the equation of motion (3.35) and recast Eq.(3.31) as

$$\rho_{\phi}(a) = V_0 \sqrt{1 - \left(1 + \frac{1}{w_0}\right) a^{-6}},$$

where w_0 is the current value of the equation of state parameter. In [111] a variable

Chaplygin gas model was proposed, noting that the tachyon field evolving in an FLRW universe can be identified with a Chaplygin gas whose parameter A ceases to be constant and becomes time-dependent $A(a)$. Related models were considered in [116,124], but presented the same shortcomings as the GCG. The possibility of building a unified model in the framework of tachyon scalar field was also considered in [105,125].

Actually, every model that attempts to unify DM and DE will face the challenges of a non-vanishing sound speed and Jeans instabilities [22], which are the sources of the tension between the theoretical predictions and the observations [126]. However these problems can be avoided if we consider the GCG as a candidate for dark energy alone[2], and that there is also usual cold dark matter in the universe [17,127].

With that in mind, throughout this work, we assume that the tachyon field is a dark energy candidate that kicks in only in recent times leading to the late-time accelerated expansion.

4.1.2 Tachyon as a DE candidate

For cosmological purposes, the typical tachyon field potential has the form [73,74,85, 107–110,128]

$$V(\phi) = m^{4-n}\phi^{-n} \tag{4.6}$$

where m is a constant with mass dimension and n is a positive constant such that for $n > 2$ the system has a dust-like attractor solution, while for $0 < n < 2$ the attractor of the dynamics corresponds to an accelerating universe [110]. The case $n = 2$, admits a scaling solution [74].

The asymptotic behavior of the inverse-power-law potential Eq. (4.6) is consistent with the original exponential potential coming from string theory, in which the rolling tachyon describes a low-energy sector for D-branes and open strings [103,110]. When the field rolls towards infinity the potential should vanish, representing the decay of D-branes in the asymptotic vacuum [58,103]. The exponential potential may be recovered

[2]The possibility of the tachyon as a candidate for dark matter was also explored, but it presented fine tuning issues or needed usual particle dark matter to prevent instabilities [104,106]

taking the appropriate limit $n \to \infty$ in Eq. (4.6).

The constant m in Eq. (4.6) can be replaced in favor of more meaningful quantities. Note that, according to Eq. (4.2) the current value of the tachyonic energy density is

$$\rho_\phi^{(0)} = \frac{V(\phi_0)}{\sqrt{1-\dot{\phi}_0^2}} = \frac{m^{4-n}\phi_0^{-n}}{\sqrt{|w_0|}},$$

where we used $w_0 = -1 + \dot{\phi}_0^2$. Therefore,

$$m^{4-n} = \rho_\phi^{(0)}\phi_0^n\sqrt{|w_0|},$$

and the potential can be written as

$$V(\phi) = \rho_\phi^{(0)}\left(\frac{\phi_0}{\phi}\right)^n\sqrt{|w_0|}. \tag{4.7}$$

Using Eq. (3.31), the scalar field energy density becomes

$$\rho_\phi(z) = \rho_\phi^{(0)}\left(\frac{\phi_0}{\phi(z)}\right)^n\sqrt{\frac{|w_0|}{1-\dot{\phi}^2(z)}}. \tag{4.8}$$

Recipe for the potential

In scalar field models for dark energy, it is always possible to find a potential which will reproduce a given evolution, since we have the liberty of trading off the scale factor $a(t)$ for the function $V(\phi)$ [109]. Under certain circumstances, such as in a scalar-field-dominated universe, it is even possible to construct an analytical expression for the potential, as we shall show. The so-called first order formalism, which relates the potential to the Hubble parameter, is discussed in [129].

The procedure is as follows [109, 128]: since $\rho \propto H^2$, differentiating the Friedmann equation (2.13) with respect to time leads to

$$2\frac{\dot{H}}{H} = \frac{\dot{\rho}}{\rho} \tag{4.9}$$

Now, we recast the continuity equation, Eq.(2.15), as

$$\frac{\dot{\rho}_\phi}{\rho_\phi} = -3H(1 + w_\phi). \tag{4.10}$$

Neglecting both matter and radiation contributions such that, in a scalar-field-dominated universe, $\rho \approx \rho_\phi$. , Eqs. (4.9) and (4.10) lead to

$$1 + w_\phi(t) = -\frac{2}{3}\frac{\dot{H}}{H^2}, \tag{4.11}$$

which is valid for any scalar field. In particular, we can rearrange the equation of state (3.33) and energy density expression (3.31) for the tachyon field,

$$\begin{cases} w_\phi = \dot{\phi}^2 - 1, \\ \rho_\phi = \frac{V(\phi)}{\sqrt{1-\dot{\phi}^2}}, \end{cases} \Rightarrow \begin{cases} \dot{\phi}^2 = 1 + w_\phi, \\ V(\phi) = \sqrt{-w_\phi}\rho_\phi, \end{cases}$$

and, using Eqs.(4.11) and (2.13), we finally arrive at

$$\phi(t) = \int \mathrm{d}t \left(-\frac{2}{3}\frac{\dot{H}}{H^2}\right)^{1/2},$$
$$V(\phi) = \frac{3H^2}{\kappa^2}\left(1 + \frac{2}{3}\frac{\dot{H}}{H^2}\right)^{1/2}.$$

Hence, for any given expansion $a(t)$ we can find how both the field and the potential evolve with time (and consequently, how the potential depends on the field itself). For instance, suppose a power-law expansion, $a(t) \propto t^p$. In this case, $\dot{H}/H^2$ is constant and, neglecting the integration constant, wet get

$$\phi(t) = \left(\frac{2}{3p}\right)^{1/2} t,$$

$$V(t) = \frac{3p^2}{\kappa^2}\left(1 - \frac{2}{3p}\right)^{1/2}\frac{1}{t^2},$$

with $p > 2/3$. In turn, the potential as a function of the field is

$$V(\phi) = \frac{2p}{\kappa^2}\left(1 - \frac{2}{3p}\right)^{1/2} \phi^{-2}.$$

The inverse-squared potential corresponds to the one that gives rise to scaling solution [73, 74]. Also, it is the tachyon counterpart of the exponential potential of quintessence. In fact, if $|\partial_\mu \phi \partial^\mu \phi| \ll 1$, the tachyonic Lagrangian can be approximated by

$$p(\phi, X) = -V(\phi)\sqrt{1 - \dot{\phi}^2} \approx \frac{\dot{\psi}^2}{2} - U(\psi),$$

with,

$$\psi = \int \mathrm{d}\phi \, \sqrt{V(\phi)}, \qquad U(\psi) = V[\phi(\psi)].$$

For the inverse-squared potential, $V(\phi) = A/\phi^2$, with A constant, the new field and potential are

$$\psi = \sqrt{A} \ln \phi, \qquad U(\psi) = A e^{-2\psi/\sqrt{A}}.$$

Curiously, in quintessence, the exponential potential also gives rise to scaling solution, and power-law expansion in the scalar-field-dominated epoch [49, 70].

4.2 Interacting tachyon model

We are interested in the expansion history of the universe when the tachyon scalar field fuels the current accelerated phase. With that in mind, we will consider a universe with radiation, visible matter (baryons), cold dark matter and tachyonic dark energy. We also let the DM and DE components interact with each other. This framework will be called Interacting Tachyon Model (ITM).

Phenomenologically, the coupling is an energy exchange between dark matter and

the scalar field, given by Eqs. (3.38) and (3.39):

$$\dot{\rho}_c + 3H\rho_c = Q, \tag{4.12}$$

$$\dot{\rho}_\phi + 3H(1+w)\rho_\phi = -Q, \tag{4.13}$$

where the coupling term, Eq. (3.40), is

$$Q = \beta(\phi)\rho_c\dot{\phi}. \tag{4.14}$$

When $Q > 0$, the energy transfer goes from DE to DM, while when $Q < 0$, the transfer occurs the other way around. We note that, since $\dot{\phi}$ might assume negative values, the sign of β is not enough to determine the direction of the interaction.

In this work we will assume that the coupling β is constant, which translates to a model where, according to Eq. (3.40), the effective mass of the dark matter particle depends on the scalar field, $M(\phi) = \bar{M}e^{-\beta\phi}$. Another interesting possibility would be a Yukawa interaction, where $M(\phi) = \bar{M} - \xi\phi$, and ξ is the coupling constant. Such coupling was explored in [85].

The coupling constant β in not dimensionless. From the definition of the Lagrangian for the tachyon Eq.(3.30), we see that $\dot{\phi}$ is dimensionless, which implies the coupling has dimension $[\beta] = (\text{mass})^1$. So, it would be interesting to rescale the coupling $\beta \to \beta' A$ using a constant A with dimension $(\text{mass})^1$. But, which scale should we pick? Note that the continuity equation for DM (4.12) can be rearranged as

$$\dot{\rho}_c + \left[3H - \beta' A\dot{\phi}\right]\rho_c = 0,$$

such that, inspecting the terms between square brackets, we see that a natural choice is $A = H_0$. Hence we will assume a coupling kernel

$$Q = \beta H_0\rho_c\dot{\phi}, \tag{4.15}$$

where now β is the dimensionless coupling constant. With this redefinition, Eq. (4.12)

becomes

$$\dot{\rho}_c = -\left[3H - \beta H_0 \dot{\phi}\right] \rho_c,$$

which yields a solution

$$\rho_c(a) = A\, a^{-3} \exp[\beta H_0 \phi(a)],$$

where A is an integration constant that can be written as function of the current values of the energy density and the field. Replacing the scale factor in favor of the redshift, the resulting expression for the cold dark matter energy density evolution coupled to a scalar field is

$$\rho_c(z) = \rho_c^{(0)}\, (1+z)^3 \exp\{\beta H_0 \left[\phi(z) - \phi_0\right]\}. \tag{4.16}$$

The equation of motion for the coupled tachyon field is found substituting the energy density Eq. (4.2) in the continuity equation (4.13), along with the coupling (4.15), resulting in

$$\ddot{\phi} = -(1-\dot{\phi}^2) \left[3H\dot{\phi} + \frac{\mathrm{d}\ln V}{\mathrm{d}\phi} - \beta H_0 \rho_c \frac{\sqrt{1-\dot{\phi}^2}}{V(\phi)}\right]. \tag{4.17}$$

Finally, using Eqs. (4.8) and (4.16), along with the usual expression for the radiation and baryon energy densities, Eq. (2.13) gives the Hubble parameter

$$H(z) = H_0 \left[\Omega_r^{(0)}(1+z)^4 + \Omega_b^{(0)}(1+z)^3 + \Omega_c^{(0)} f_c(z) + \Omega_\phi^{(0)} f_\phi(z)\right]^{1/2}, \tag{4.18}$$

where

$$f_c(z) = (1+z)^3 \exp\{\beta H_0 \left[\phi(z) - \phi_0\right]\},$$
$$f_\phi(z) = \left[\frac{\phi_0}{\phi(z)}\right]^n \sqrt{\frac{|w_0|}{1-\dot{\phi}^2(z)}}.$$

The energy density parameter for the scalar field satisfies the constraint

$$\Omega_\phi^{(0)} = 1 - \Omega_r^{(0)} - \Omega_b^{(0)} - \Omega_c^{(0)},$$

and ϕ and $\dot{\phi}$ are the solutions for the equation of motion (4.17). The Friedmann equation (4.18) gives the expansion history of the universe. The cosmological parameters that define the model are the Hubble constant H_0 (parameterized by h defined via $H_0 = 100h\,\mathrm{km\,s^{-1}\,Mpc^{-1}}$), the dimensionless density parameter for radiation $\Omega_r^{(0)}$ (given by Eq. (2.37) as function of T_{CMB} and N_{eff}), baryons $\Omega_b^{(0)}$ and dark matter $\Omega_c^{(0)}$, the current values of the field ϕ_0 and the equation of state parameter of dark energy w_0, and the coupling constant β.

Since we are interested in constraining the present values of the cosmological parameter, it is convenient to solve the equation of motion for the field, Eq. (4.17), using the redshift z instead of cosmic time t, via the transformation $\mathrm{d}t = -\left[(1-z)H(z)\right]^{-1}\mathrm{d}z$. In this approach using the current values of ϕ_0 and $\dot{\phi}_0 = \sqrt{1+w_0}$ as initial conditions[3] is straightforward, eliminating the need for a shooting method to infer the initial conditions from the boundary values.

From the set of free parameters, the ones that affect the most the scalar field evolution are, obviously, ϕ_0, w_0 and β. The behavior of the tachyon field, i.e. if is acts like dust or dark energy, is summarized by the equation of state $w(z) = \dot{\phi}^2 - 1$. In Fig. (4.1) we show $w(z)$ for a different values of ϕ_0, w_0 and β assuming the following fiducial cosmology:

$$(h, \Omega_b^{(0)}h^2, \Omega_c^{(0)}h^2, \phi_0 H_0, w_0, \beta) = (0.7, 0.02, 0.13, 1, -0.95, 0). \tag{4.19}$$

We see that for initial conditions that match the current state of the universe, i.e., late-time accelerated expansion, the field is effectively a matter component, with $w(z) \approx 0$, for redshifts greater than ~ 2. The main effect of different initial conditions is a shift in the transition epoch, when the tachyon freezes and starts sourcing the expansion (see also Fig. (4.2), the deceleration parameter, defined in Eq. (2.18), as function of the redshift).

The concordance model ΛCDM fits the expansion history remarkably well, hence we

[3]Since $\dot{\phi}^2 = 1+w$, there is also the possibility of $\dot{\phi}_0 = -\sqrt{1+w_0}$. We are interested solutions with late-time inflation, so usually $w_0 \sim -1$, implying $\dot{\phi} \sim 0$, hence, the sign doesn't really matter.

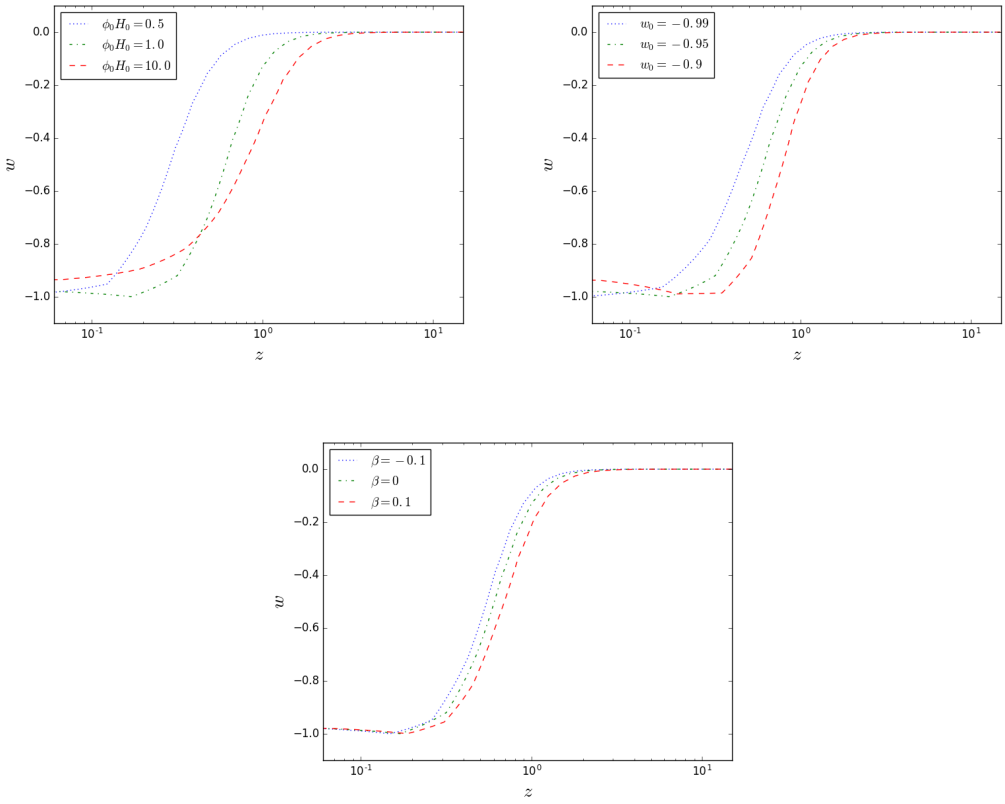

Figure 4.1: Evolution of the tachyonic equation of state. The cosmological parameters, except the ones being varied, are fixed with the fiducial values (4.19).

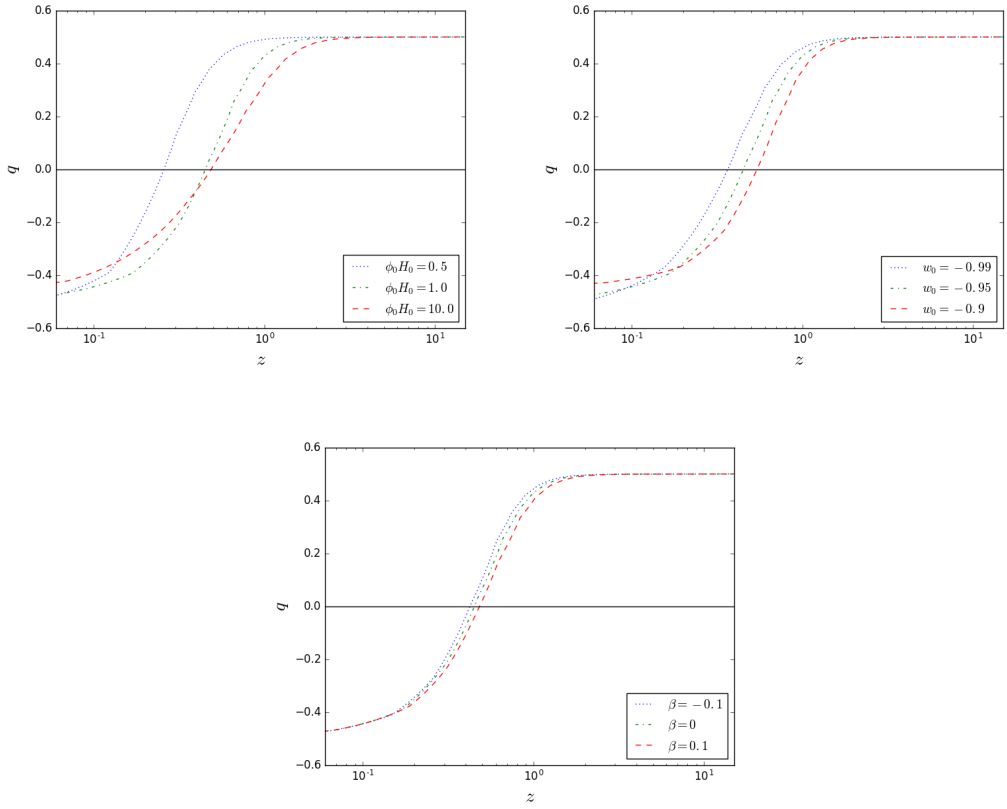

Figure 4.2: Deceleration parameter q as function of the redshift z.The cosmological parameters, except the ones being varied, are fixed with the fiducial values (4.19).

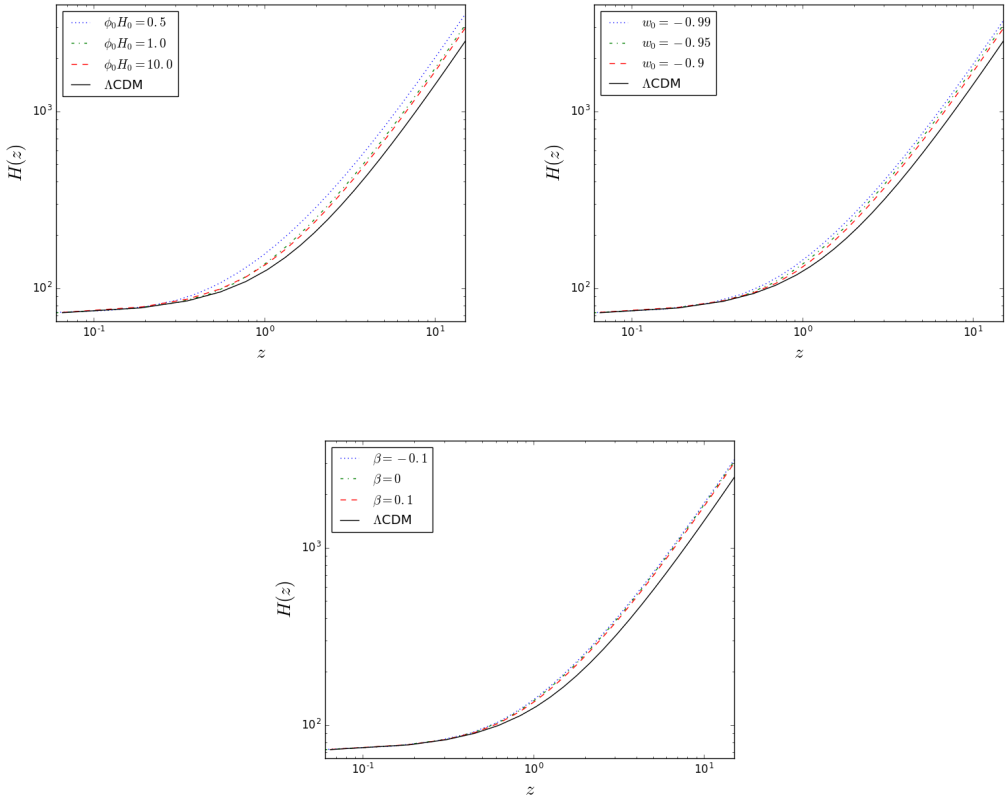

Figure 4.3: Hubble diagrams for the ITM model with several initial conditions and the standard ΛCDM. The cosmological parameters, except the ones being varied, are fixed with the fiducial values (4.19).

do not expect a cosmologically viable alternative to depart much from it. In Fig. (4.3) we present the Hubble parameter as function of the redshift for different initial conditions for the tachyon model and the baseline ΛCDM counterpart. As noted above, in the matter epoch the field acts like dust, enhancing the matter content of the universe. In all scenarios depicted in Fig. (4.3), the tachyon model predicts a higher value for $H(z)$ at high-z. To reproduce the cosmological constant scenario in the high-z region, we would need a mismatch in the low-z region, requiring a lower H_0.

Indeed, there is a subset of initial conditions at $z = 0$ which successfully reproduces the history of the universe. From Fig. (4.4) we note that if ϕ_0, w_0 e β are rather small, the ratio $r = \rho_c/\rho_\phi$ turns out to be less than unit in the matter epoch, meaning that the standard matter-dominated epoch is suppressed in favor of a tachyon matter epoch. That is not an attractive feature since we are assuming that the tachyonic field a DE candidate that dominates the energy content at late times but leave the matter epoch

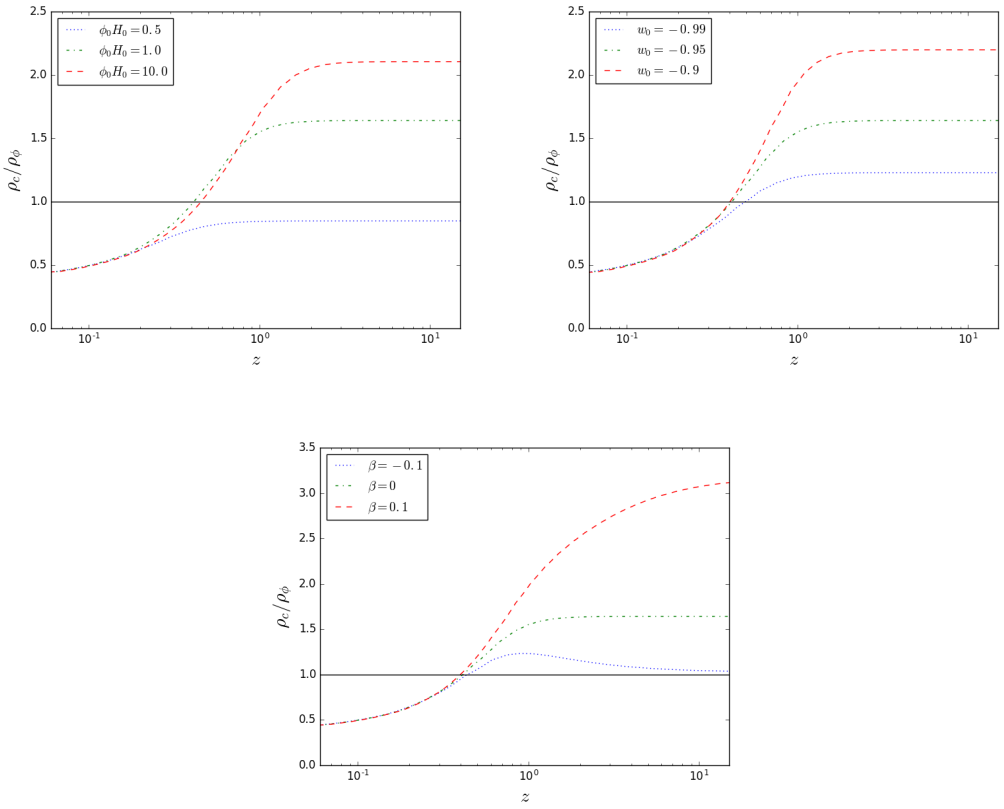

Figure 4.4: Evolution of the ratio $r = \rho_c/\rho_\phi$. The cosmological parameters, except the ones being varied, are fixed with the fiducial values (4.19).

somewhat unaffected.

Chapter 5

Observational constraints

In this chapter, we will discuss how to constraint cosmological parameters using the observational information and how to compare different models in an approximate fashion. Then the compilation of data will be presented. Finally, we'll report the main results of our analysis.

5.1 Methodology

5.1.1 Parameter Estimation

Suppose that a given physical quantity x, described by a given theoretical model, has a probability density function (PDF) $f(x;\theta)$, which depends on an unknown parameter θ. That function tells us the probability of measuring x given the theoretical parameter θ. If we perform N independent measurements x, the joint probability of getting each x_i in an interval $\mathrm{d}x_i$ around x_i is given by

$$f(\{x_i\};\theta)\,\mathrm{d}^N x_i = \prod_i f(x_i;\theta)\,\mathrm{d}x_i$$

and $f(\{x_i\};\theta)$ is called the *likelihood function*, represented by $\mathcal{L}(\mathbf{x};\theta)$ [17]. If the measurements are not independent of each other the joint probability could be more complicated, not being the simple product of each PDF since the experimental points are correlated to one another, although the meaning of the likelihood function stays

the same. Furthermore, if the model is described by more than one parameter, say, D parameters, the likelihood function is generalized in a D-dimensional parameter space as $\mathcal{L}(\mathbf{x};\theta)$, where $\theta = (\theta_1, \ldots, \theta_D)$. Hence, the likelihood function gives the probability that a given experiment would get the data it did, given a theory, and it allows us to estimate the parameters and the respective uncertainties [3].

Naturally, our best guess for the value of the parameters is the set that maximizes the likelihood function, that is, the one that has the greatest likelihood to reproduce the measured results, maximizing the agreement between model and observation. This method is called *maximum likelihood estimative*. Therefore, we define the best estimators $\hat{\theta}_i$ as the parameters that satisfy

$$\left.\frac{\partial \mathcal{L}(\mathbf{x};\theta)}{\partial \theta_i}\right|_{\theta_i=\hat{\theta}_i} = 0, \qquad i = 1, \ldots, D.$$

Since each $\hat{\theta}_i$ is dependent on the data set $\mathbf{x}$, it is a random variable that has a mean value and variance. It can be arduous to find analytical solutions, though. In order to get the distribution of $\hat{\theta}_i$, one could embrace the frequentist approach, simulating a number of data sets using the original distribution and drawing the parameters estimate from it, but that, generally, is numerically expensive. However, the biggest limitation of the maximum likelihood approach is that it completely ignores our previous knowledge regarding the parameters. Any preceding information, for instance, the result of a past experiment or a parameter whose value must lie within a given physical range, is not taken into account. In cosmology and astrophysics, one can not afford to neglect this kind of knowledge since making new observations can be costly, there isn't much data to work with and the parameters are usually strongly correlated. Any piece of evidence must be taken into account.

That is when the *Bayesian statistics* comes to our rescue. Instead of looking at the probability of *getting the data given the parameters*, let us focus on the probability of *getting the parameters given the data*, something that can be done by means of a

well-known result from probability theory, the so-called *Bayes' theorem*:

$$p(A|B,I) = \frac{p(B|A,I)p(A|I)}{p(B|I)}, \tag{5.1}$$

where $P(X|Y,I)$ reads 'the probability that the hypothesis X is true given that the hypothesis Y and I also are true' [130]. Here, I represents any other relevant background information that we assume is true. In order to understand Eq. (5.1) note that since

$$p(A,B|I) = p(A|B,I)p(B|I),$$

that is, the joint probability of A and B is the probability of A given B times the probability of B (always conditioned to the background information), and that, of course, $p(A,B|I) = p(B,A|I)$, Eq. (5.1) follows.

Translating to the problem of estimating the parameters of a model, we represent the parameters θ by A, the data $\mathbf{x}$ by B and restate the theorem as

$$p(\theta|\mathbf{x}) = \frac{p(\mathbf{x}|\theta)p(\theta)}{p(\mathbf{x})},$$

where, for simplicity's sake, from now on we will omit the background information I, but we have to always keep in mind that we are dealing with conditional probabilities.

The L.H.S., $p(\theta|\mathbf{x})$ is the *posterior probability* of the parameters given the observations, which is proportional to the likelihood function $p(\mathbf{x}|\theta)$ times a *prior probability* $p(\theta)$ that express the knowledge about the parameters prior to the observation. The function $p(\mathbf{x})$ is called the *evidence* and, for parameter inference purposes, can be regarded as a normalization, since it does not depend on θ,

$$p(\mathbf{x}) = \int \mathrm{d}\theta\, p(\mathbf{x}|\theta)p(\theta), \tag{5.2}$$

although it is important in the context of *model selection* when we are interested in comparing different theoretical propositions and assessing which is preferable by to the data [131].

Thus, the posterior contains the information we wanted, namely, the probability distribution of the parameters given that we have a data set and that we also have some prior information about it. Now we are left to find the best estimators $\hat{\theta}_i$ maximizing $p(\theta|\mathbf{x})$,

$$\left.\frac{\partial p(\theta|\mathbf{x})}{\partial \theta_i}\right|_{\theta_i=\hat{\theta}_i} = 0, \qquad i = 1, \ldots, D. \tag{5.3}$$

In general, the set of parameters that maximizes the posterior will be different than the one that maximizes the likelihood, since now we have the priors, although this distinction might be diluted as we update the posterior with new data that has discriminatory power [3].

From the normalized posterior, one can define confidence regions $R(\alpha)$ for the estimated parameters. Such regions quantify our *degree of belief* in the estimate, and are defined as the smallest $R(\alpha)$ that satisfies

$$\int_{R(\alpha)} \mathrm{d}^D\theta_i \, p(\theta|\mathbf{x}) = \alpha, \tag{5.4}$$

with $0 < \alpha < 1$. Typically, we choose $\alpha = 0.68, 0.95, 0.99$ which represents the 1σ, 2σ, 3σ confidence regions.

Now, if our interest is focused on a given parameter, or conversely, we do not care about the distribution of a given *nuisance* parameter, we turn to the process of *marginalization*, which consists of integrating the posterior over the parameters that are not important to us, leaving only the desired marginalized probability density function. For instance, suppose $\theta = (\theta_1, \theta_2)$, and the critical value is θ_1. So, if θ_2 is a positive nuisance parameter, the posterior marginalized over θ_2 is

$$p(\theta_1|\mathbf{x}) = \int_0^\infty \mathrm{d}\theta_2 \, p(\theta_1, \theta_2|\mathbf{x}).$$

From $p(\theta_1|\mathbf{x})$, it is possible to find a new estimate to θ_1 and its marginalized confidence limits. It could be, for instance, the mean value

$$\langle\theta_1\rangle = \int \mathrm{d}\theta_1 \, \theta_1 \, p(\theta_1|\mathbf{x}),$$

with confidence limits given by Eq. (5.4), or even another suitable statistical estimate.

In cosmological applications, the observational data is usually Gaussian distributed. Even when the errors in each measurement are stochastic but not Gaussian the sum of many independent random errors tend to be normally distributed, due to the *central limit theorem* [132]. The likelihood function for a single, Gaussian distributed, measurement is

$$\mathcal{L}(x;\theta) = \frac{1}{\sqrt{2\pi\sigma}} \exp\left\{ -\frac{1}{2}\left(\frac{x^{th} - x^{obs}}{\sigma_x} \right)^2 \right\},$$

where x^{th} stands for the theoretical prediction, given the parameters θ, for the measurement, and x^{obs} is the measured point itself with an associated standard deviation σ_x. Hence, the joint likelihood for N measurements, $\mathbf{x} = (x_1, \ldots, x_N)$ is given by

$$\begin{aligned}
\mathcal{L}(\mathbf{x};\theta) &= \prod_{i=1}^{N} \frac{1}{\sqrt{2\pi\sigma_{x_i}}} \exp\left\{ -\frac{1}{2}\left(\frac{x_i^{th} - x_i^{obs}}{\sigma_{x_i}} \right)^2 \right\}, \\
&= \left(\prod_{i=1}^{N} \frac{1}{\sqrt{2\pi\sigma_{x_i}}} \right) \exp\left\{ -\frac{1}{2} \sum_{i=1}^{N} \left(\frac{x_i^{th} - x_i^{obs}}{\sigma_{x_i}} \right)^2 \right\}.
\end{aligned}$$

We often employ the shorthand notation $\mathcal{L} = \mathcal{L}_0 \exp\left(-\chi^2/2\right)$, where

$$\chi^2 = \sum_{i=1}^{N} \left(\frac{x_i^{th} - x_i^{obs}}{\sigma_{x_i}} \right)^2$$

is the so-called *chi-squared* function. To maximize the likelihood function is equivalent to minimize the χ^2 function. Thus, the best-fit values for the parameters of a given model, given an experimental data set, are the estimators $\hat{\theta}_j$ that maximize the posterior, hence the likelihood (at least for flat priors), which in turn corresponds to the minimum chi-squared.

Unfortunately, evaluating the posterior might also be cumbersome. Often we do not have analytical solutions, therefore an efficient numerical method to explore the parameter space is needed. In this context, the Monte Carlo Markov Chain (MCMC) technique comes in handy. The method consists of drawing samples from the posterior, building a sequence (called chain) whose elements are chosen in a random fashion and each point depends only on the previous one [133]. The crucial property of Markov

chains is that they can be shown to converge to a stationary state where successive elements of the chain are samples from the target distribution, in our case the posterior $p(\theta|\mathbf{x})$ [130].

So, in this way one can numerically estimate the parameters of a given model, taking into account all the experimental data at hand and every piece of previous information, and quantify the degree of belief in the obtained results.

5.1.2 Information Criterion

Given the large number of theoretical candidates to dark energy, it is interesting to have a method to compare the merits of different proposals. One such method to compare two models uses the evidence integral Eq. (5.2) to compute the Bayes factor, which is a measure of the support in favor of one model versus the other given the observed data [132]. Computing the Bayesian evidence, on the other hand, usually is not an easy task. Hence, it is useful to have methods that approximate models selection under suitable assumptions and simplifications. These are collectively called *information criteria*.

To fit a given model to a set of observations we employ the maximum likelihood method, which consists of finding the parameters that maximize the likelihood function (or minimize the chi-squared function), hence, a naive method would be to compare the best-fit χ^2 at face value. However, this analysis can be misleading, since candidates may have different numbers of free parameters, and models with more free parameters, usually, result in a smaller χ^2 (at the cost of complexity). So it is useful to employ an information criterion method to quantify the quality of the fit including a penalty term for more complex models. Two of the most widespread criteria are the Akaike Information Criterion (AIC) [134] and the Bayesian Information Criterion (BIC) [135]. These are respectively defined as

$$\mathrm{AIC} = -2\ln\mathcal{L}_{\max} + 2k, \tag{5.5}$$

$$\mathrm{BIC} = -2\ln\mathcal{L}_{max} + k\ln N, \tag{5.6}$$

where $\mathcal{L}_{max}$ is the maximum likelihood function, k is the number of model parameters and N denotes the total number of observational points used in the analysis. If the data points are described by a Gaussian PDF, then

$$\chi^2_{min} = -2 \ln \mathcal{L}_{max}.$$

In principle, the lower the value of the information criterion, the better the model under consideration explain the data. It is more useful, though, to introduce a reference scenario and compare different models with respect to it. Hence, for any given model M, we define the relative difference to the reference model REF as

$$\Delta X = X_M - X_{REF}$$

where $X = AIC$ or BIC. As a rule of thumb, one might conclude that [136, 137]:

(i) if $\Delta X \leq 2$, then the model under consideration has substantial support with respect to the reference model,

(ii) if $4 \leq \Delta X \leq 7$ then the model has less support with respect to the reference model, and finally,

(iii) if $\Delta X \geq 10$ then the model essentially has no support.

It is customary to choose as reference the model with the lower value of information criterion. Naturally, in cosmological applications, we usually choose the concordance ΛCDM model.

The main difference between AIC and BIC is that the latter penalizes models with more free parameters more harshly than the former.

5.2 Data sets

Here we present the data compilation employed in this work. We use a combination of late-time ($z < 2$) Hubble parameter, type IA supernovae, baryon acoustic oscillations

measurements and early-time CMB observations in order to constrain the cosmological parameters.

5.2.1 Cosmic Chronometers

The cosmic chronometer (CC) approach, first introduce in Ref. [138], is a powerful implementation to measure the Hubble parameter. The method determines $H(z)$ using the relative ages of the most massive, passively evolving early-type galaxies. In an FLRW universe, the Hubble parameter can be expressed as

$$H(z) = -\frac{1}{1+z}\frac{\mathrm{d}z}{\mathrm{d}t},$$

hence, by measuring the quantity dz/dt, one can directly measure $H(z)$ in a given redshift.

Cosmic chronometers are able to impose constraints on cosmological parameters that are as good as the ones coming from "standard" probes, such as BAO and SNe, with the upside that it provides a direct measurement of the expansion rate $H(z)$ without any previous assumption about the cosmological model (besides isotropy and homogeneity) [139]. It is important to note that there are no correlations between CC and anisotropic BAO data. Another interesting feature of CC measurements is that they are extremely useful in constraining models with dynamical dark energy equation of state and for models where CMB constraints show parameter degeneracies with the expansion history [139]. For an extensive discussion on the implementation of CC data, sources of uncertainties and overall difficulties of the method, see Ref. [140].

Here we consider a recent compilation of cosmic chronometers as provided in [141]. The data set contains 30 measurements of $H(z)$ obtained using the CC approach [140–146] in the redshift range $0 < z < 2$, which covers roughly 10 Gyr of cosmic time. The data set is listed in Tab. 5.1.

The χ^2 for the $H(z)$ data is given by

$$\chi^2_{\rm CC} = \left[\frac{H^{th}(z) - H^{obs}(z)}{\sigma_{H(z)}}\right]^2 \tag{5.7}$$

where $H^{th}(z)$ is the theoretical Hubble parameter, $H^{obs}(z)$ and $\sigma_{H(z)}$ are the observed Hubble parameter and its standard deviation, respectively.

Table 5.1: Observed Hubble parameters $H(z)$ in $[\mathrm{km\,s^{-1}Mpc^{-1}}]$ obtained using the cosmic chronometer (CC) technique. This compilation was presented in [141].

z	$H(z)$	Ref.	z	$H(z)$	Ref.
0.07	69.0 ± 19.6	[142]	0.4783	80.9 ± 9.0	[141]
0.09	69.0 ± 12.0	[143]	0.48	97.0 ± 62.0	[144]
0.12	68.6 ± 26.2	[142]	0.5929	104.0 ± 13.0	[140]
0.17	83.0 ± 8.0	[145]	0.6797	92.0 ± 8.0	[140]
0.1791	75.0 ± 4.0	[140]	0.7812	105.0 ± 12.0	[140]
0.1993	75.0 ± 5.0	[140]	0.8754	125.0 ± 17.0	[140]
0.2	72.9 ± 29.6	[142]	0.88	90.0 ± 40.0	[144]
0.27	77.0 ± 14.0	[145]	0.9	117.0 ± 23.0	[145]
0.28	88.8 ± 36.6	[142]	1.037	154.0 ± 20.0	[140]
0.3519	83.0 ± 14.0	[140]	1.3	168.0 ± 17.0	[145]
0.3802	83.0 ± 13.5	[141]	1.363	160.0 ± 33.6	[146]
0.4	95.0 ± 17.0	[145]	1.43	177.0 ± 18.0	[145]
0.4004	77.0 ± 10.2	[141]	1.53	140.0 ± 14.0	[145]
0.4247	87.1 ± 11.2	[141]	1.75	202.0 ± 40.0	[145]
0.4497	92.8 ± 12.9	[141]	1.965	186.5 ± 50.4	[146]

5.2.2 Type Ia Supernovae

In this work we use the data from the Joint Light-curve Analysis (JLA) [19], a joint analysis of type Ia supernovae obtained by Sloan Digital Sky Survey (SDSS-II) and Supernova Legacy Survey (SNLS). The full data set totals 740 spectroscopically confirmed SNIa and high-quality light curves from the full 3-year SDSS survey and also from SNLS, Hubble Space Telescope (HST) and several nearby experiments. In our analysis we actually use a compressed form of the JLA likelihood [1], consisting of 31 control points $(\mathbf{z_b}, \mu_\mathbf{b})$ of the distance modulus as function of the redshift, that en-

[1] An electronic version of the data, including the covariance matrix, can be downloaded at `http://supernovae.in2p3.fr/sdss_snls_jla/ReadMe.html`. Also, the covariance matrix is presented in Tab. F2 of Ref. [19].

capsulate most of its information in an accurate way. The binned supernovae data is presented in Tab. (5.2).

The χ^2 for the SNe data is given by

$$\chi^2_{\rm SNe} = r_i C_b^{-1}(r_i, r_j) r_j, \tag{5.8}$$

where

$$r_i = \mu_{b,i} - M - 5\log_{10} d_L(z_{b,i}, \theta),$$

M is a normalization parameter that should be fitted along with the cosmological parameters θ, d_L is the luminosity distance, defined in Eq. (2.46), and C_b is the covariance matrix of μ_b.

Table 5.2: Binned distance modulus fitted to the JLA sample.

z_b	μ_b	z_b	μ_b	z_b	μ_b
0.010	32.9538	0.051	36.6511	0.257	40.5649
0.012	33.8790	0.060	37.1580	0.302	40.9052
0.014	33.8421	0.070	37.4301	0.355	41.4214
0.016	34.1185	0.082	37.9566	0.418	41.7909
0.019	34.5934	0.097	38.2532	0.491	42.2314
0.023	34.9390	0.114	38.6128	0.578	42.6170
0.026	35.2520	0.134	39.0678	0.679	43.0527
0.031	35.7485	0.158	39.3414	0.799	43.5041
0.037	36.0697	0.186	39.7921	0.940	43.9725
0.043	36.4345	0.218	40.1565	1.105	44.5140
				1.300	44.8218

5.2.3 Baryon Acoustic Oscillations

We employ a total of 7 data points from the following BAO collaborations: 6dF Galaxy Survey (6dF) [147], Sloan Digital Sky Survey's Main Galaxy Sample (SDSS-MGS) [148], Baryon Oscillation Spectroscopic Survey's LOWZ and CMASS galaxy samples (BOSS-LOWZ and BOSS-CMASS, respectively) [149], and WiggleZ Dark Energy Survey (WiggleZ) [150]. WiggleZ's data is correlated and we take it into account [2]. These measurements and their corresponding effective redshift z_{eff} are summarized in

[2]The inverse covariance matrix for the WiggleZ data can be found in Table 4 in Ref. [150].

Tab. 5.3. Defining the relative BAO distance

$$r_{\rm BAO} = \frac{D_V(z)}{r_s(z_d)},$$

the χ^2 for the BAO data is given by

$$\chi^2_{\rm BAO} = \bar{\chi}^2_{\rm BAO} + \chi^2_{\rm WiggleZ}, \tag{5.9}$$

where

$$\bar{\chi}^2_{\rm BAO} = \left[\frac{r^{th}_{\rm BAO}(z_{eff}) - r^{obs}_{\rm BAO}(z_{eff})}{\sigma_{r_{\rm BAO}}}\right]^2$$

gives the likelihood function for the uncorrelated BAO measurements (6dF, SDSS-MGS, BOSS-LOWZ and BOSS-CMASS), $r^{th}_{\rm BAO}(z_{eff})$ is the theoretical BAO distance, $r^{obs}_{\rm BAO}(z_{eff})$ and $\sigma_{r_{\rm BAO}}$ are the observed distance and its standard deviation, respectively, and

$$\chi^2_{\rm WiggleZ} = (r^{th}_{{\rm BAO},i} - r^{obs}_{{\rm BAO},i}) C^{-1}_{\rm WiggleZ}(r_{{\rm BAO},i}, r_{{\rm BAO},j})(r^{th}_{{\rm BAO},j} - r^{obs}_{{\rm BAO},j})$$

is the likelihood for the WiggleZ data.

Table 5.3: The low redshift BAO data.

z_{eff}	Measurement	Experiment	Ref.
0.106	$r_s/D_V = 0.336 \pm 0.015$	6dF	[147]
0.15	$D_V/r_s = (664 \pm 25)/152.66$	SDSS-MGS	[148]
0.32	$D_V/r_s = (1264 \pm 25)/153.19$	BOSS-LOWZ	[149]
0.44	$D_V/r_s = (1716.4 \pm 83)/152.3$	WiggleZ	[150]
0.57	$D_V/r_s = (2056 \pm 25)/153.19$	BOSS-CMASS	[149]
0.6	$D_V/r_s = (2220.8 \pm 101)/152.3$	WiggleZ	[150]
0.73	$D_V/r_s = (2516.1 \pm 86)/152.3$	WiggleZ	[150]

5.2.4 Cosmic Microwave Background

For the CMB data, we use the distance priors from the Planck Collaboration 2015 Data Release (Planck15) [31], listed in Tab. 5.4, together with their normalized covariance (or correlation) matrix. The covariance matrix C in terms of the correlation matrix D is given by $C(p_i, p_j) = C_{ij} = \sigma_i \sigma_j D_{ij}$ (without summation), where σ_i is the standard

deviation of parameter i. Then, the χ^2 for the CMB data is given by

$$\chi^2_{\rm CMB} = (p_i^{th} - p_i^{obs}) C^{-1}_{\rm CMB}(p_i, p_j)(p_j^{th} - p_j^{obs}) \tag{5.10}$$

where p^{th} and p^{obs} denotes the theoretical and observational distance priors, respectively, and the vector $\mathbf{p}$ is defined as $\mathbf{p} = (R, \ell_A, \Omega_b^{(0)} h^2)$.

Table 5.4: The Planck15 [31] distance priors and the normalized covariance matrix.

		R	ℓ_A	$\Omega_b^{(0)} h^2$
R	1.7382 ± 0.0088	1	0.64	-0.75
ℓ_A	301.63 ± 0.15	0.64	1	-0.55
$\Omega_b^{(0)} h^2$	0.02262 ± 0.00029	-0.75	-0.55	1

5.2.5 Local value of the Hubble constant

A recent improvement in the measurement and analysis of Cepheid variables and nearby supernovae by the HST [11] reduced the uncertainty in the determination of the current value of the Hubble parameter from 3.3% to 2.4%, yielding an estimative of

$$H_0^{obs} = 73.24 \pm 1.74\,{\rm km\,s^{-1}\,Mpc^{-1}},$$

including both statistical and systematic errors. We note that, with this recent data, the tension between the direct local measurement and the model-dependent value inferred from the CMB has been raised to more than 3σ.

Nevertheless, we add this new measurement to our analysis. The χ^2 for the local H_0 data is given by

$$\chi^2_{H_0} = \left[\frac{H_0^{th} - H_0^{obs}}{\sigma_{H_0}}\right]^2, \tag{5.11}$$

where H_0^{th} is the theoretical prediction σ_{H_0} is the 1σ uncertainty.

5.3 Results

We developed a numerical code that solves the background cosmological equations and extracts the cosmological parameters with the help of an MCMC engine. We sampled the distribution of the parameters with the public `Python` package `emcee` [151], and using the maximum likelihood method we compared the theoretical predictions with a data set that comprises CC, SNe, BAO, CMB and H_0 measurements. The MCMC chains totals $\mathcal{O}(10^6)$ samples and the convergence was monitored with the Gelman and Rubin criterion [152], making sure that $R - 1 < 0.03$. The statistical analysis was performed using the `GetDist` package [3].

First we sample the parameters of the interacting tachyon model (ITM). Then, in order to assess how the ITM fits the cosmological scenario, we also draw samples for the concordance ΛCDM model Eq. (2.41), and other DE alternatives, namely, wCDM Eq. (3.17), and the interacting dark energy models IDE1 and IDE2 (3.44).

Since we are interested only in the expansion history, the crucial function in our analysis is the Hubble parameter as function of the redshift,

$$H(z) = H_0 \left[\Omega_r^{(0)}(1+z)^4 + \Omega_b^{(0)}(1+z)^3 + \Omega_c^{(0)} f_c(z) + \Omega_{de}^{(0)} f_{de}(z)\right]^{1/2}, \tag{5.12}$$

where the functions $f_c(z)$ and $f_{de}(z)$ describe how dark matter and dark energy, respectively, depend on the redshift. For the models under consideration, these functions are summarized in Tab. (5.5).

Table 5.5: The characteristic functions $f_c(z)$ and $f_{de}(z)$ for the models under consideration. These functions dictate how the cold dark matter and dark energy components evolve with redshift. In this work we choose a tachyon potential with $n = 2$.

	$f_c(z)$	$f_{de}(z)$
ΛCDM	$(1+z)^3$	1
wCDM	$(1+z)^3$	$(1+z)^{3(1+w_0)}$
IDE1	$(1+z)^3$	$\frac{\beta}{\beta+w_0}(1+z)^3 + \left(1-\frac{\beta}{\beta+w_0}\right)(1+z)^{3(1+w_0+\beta)}$
IDE2	$\frac{\beta}{\beta+w_0}(1+z)^{3(1+w_0)} + \left(1-\frac{\beta}{\beta+w_0}\right)(1+z)^{3(1-\beta)}$	$(1+z)^{3(1+w_0)}$
ITM	$(1+z)^3 \exp\{\beta H_0 [\phi(z) - \phi_0]\}$	$\left[\frac{\phi_0}{\phi(z)}\right]^n \sqrt{\frac{\lvert w_0\rvert}{1-\dot{\phi}^2(z)}}$

[3] Available at `https://github.com/cmbant/getdist`.

The parameter space of the ITM model is spanned by $\theta_{\rm ITM} = (H_0, \Omega_b^{(0)}, \Omega_c^{(0)}, \phi_0, w_0, \beta)$. We choose a tachyon potential, Eq. (4.7), with $n = 2$, such that in a dark-energy dominated epoch the universe will experience a power-law expansion.

For the other models, the free cosmological parameters are: $\theta_{\Lambda\rm CDM} = (H_0, \Omega_b^{(0)}, \Omega_c^{(0)})$ for ΛCDM, $\theta_{w\rm CDM} = (H_0, \Omega_b^{(0)}, \Omega_c^{(0)}, w_0)$ for the wCDM, and $\theta_{\rm IDE} = (H_0, \Omega_b^{(0)}, \Omega_c^{(0)}, w_0, \beta)$ for both IDE models.

To reduce the degeneracy between H_0 and the density parameters Ω_i, we actually sample h and $\Omega_i^{(0)} h^2$, where h is defined as $H_0 = 100h\,\mathrm{km\,s^{-1}Mpc^{-1}}$.

The present energy density of radiation in negligible compared to matter and dark energy. Even tough we include its contribution $\Omega_r^{(0)}$ to the Hubble expansion, Eq. (5.12), we fix $T_{CMB} = 2.7255\,\mathrm{K}$ [7], and $N_{eff} = 3.046$. Hence, from Eq. (2.37), we assume

$$\Omega_r^{(0)} h^2 = 4.1788 \times 10^{-5}.$$

Since the measurements are reportedly Gaussian distributed, the joint likelihood function is $\mathcal{L} \propto e^{-\chi^2/2}$, with

$$\chi^2(\theta, M) = \chi^2_{\rm CC}(\theta) + \chi^2_{\rm SNe}(\theta, M) + \chi^2_{\rm BAO}(\theta) + \chi^2_{\rm CMB}(\theta) + \chi^2_{H_0}(\theta), \tag{5.13}$$

where $\chi^2_{\rm CC}$ is given by Eq. (5.7), $\chi^2_{\rm SNe}$ is given by Eq. (5.8), $\chi^2_{\rm BAO}$ is given by Eq. (5.9), $\chi^2_{\rm CMB}$ is given by Eq. (5.10), and finally $\chi^2_{H_0}$ is given by Eq. (5.11).

We considered flat priors for all the parameters. In the tachyonic case, the allowed ranges of all parameters, but the current value of the equation of state of dark energy w_0, were wide enough such that further increasing it had no impact on the results. The lower bound for w_0 was set by the requirement that the tachyon is not a phantom field ($w > -1$). The range for ϕ_0 was set based on the expectation that $\phi_0 H_0 \sim 1$ [107]. These priors are summarized in Tab. (5.6). For the other models, see Tab. (5.7).

Our constraints on cosmological parameters of the interacting tachyon model are summarized in Tab. 5.8. There is a considerable difference between the best-fit value and the mean of the marginalized distribution for the present value of the field ϕ_0

Table 5.6: Flat prior distributions for the parameters of the interacting tachyon model.

Parameter	Prior distribution
M	$[24, 26]$
h	$[0.55, 0.8]$
$\Omega_b^{(0)}h^2$	$[0.01, 0.03]$
$\Omega_c^{(0)}h^2$	$[0.01, 0.3]$
$\phi_0 H_0$	$[0, 10]$
w_0	$[-1, -0.7]$
β	$[-1, 1]$

Table 5.7: Flat prior distributions for the parameters of the other DE models.

Parameter	Prior distribution
M	$[24, 26]$
h	$[0.55, 0.8]$
$\Omega_b^{(0)}h^2$	$[0.01, 0.03]$
$\Omega_c^{(0)}h^2$	$[0.01, 0.3]$
w_0	$[-1.3, -0.7]$
β	$[-1, 1]$

and the coupling constant β, which indicates that there are degeneracies among the parameters of the model. This is evidenced in the 2-dimensional marginalized posterior distribution, Fig. (5.1). Actually, we see that ϕ_0 is degenerated with both w_0 and β. Note that these are the three parameters that characterize the behavior of the scalar field.

An interacting model where the coupling was implemented using a Yukawa term between the tachyon scalar and the fermionic dark matter was proposed in Ref. [85]. There, the coupling function $\beta(\phi)$ instead of being constant, like in our proposal, was given by $\beta(\phi) = \xi/(\bar{M} - \xi\phi)$, where $\bar{M}$ is the bare mass of the fermion and ξ is the coupling constant. Despite the meager differences in the coupling kernel, our results improve the constraints on the coupling constant and on the current value of the field. In their results, the marginalized distribution for the coupling constant was unbounded from below, while for $\phi_0 H_0$ it had no upper limit. The improvement might be due to the use of a more complete and recent compilation of observational points. Notably, in their previous analysis the only information about the CMB spectra was the shift parameter R from the 3-year WMAP results, while here we employed, in addition to

Table 5.8: Best-fit values and marginalized constraints on the nuisance JLA parameter M and on the cosmological parameters h, $\Omega_b^{(0)}h^2$, $\Omega_c^{(0)}h^2$, ϕ_0, w_0 and β at 68% confidence level for the interacting tachyon model. The bottom panel presents the derived parameters $\phi_0 H_0$ and Ω_ϕ. When the upper and lower limits are equal we report the uncertainty in the last digits by the numbers between parentheses, corresponding to one standard deviation.

Parameter	Best fit	68% limits
M	24.937	$24.955^{0.023}_{-0.022}$
h	0.6821	$0.6787^{0.0056}_{-0.0051}$
$\Omega_b^{(0)}h^2$	0.02279	0.02276(26)
$\Omega_c^{(0)}h^2$	0.1173	$0.1174^{0.0014}_{-0.0012}$
ϕ_0	0.037	$0.064^{+0.061}_{-0.043}$
w_0	-0.982	$-0.984^{0.005}_{-0.016}$
β	0.132	$0.053^{0.058}_{-0.079}$
$\phi_0 H_0$	2.5	$4.3^{+1.2}_{-2.6}$
$\Omega_\phi^{(0)}$	0.6989	$0.6956^{+0.0060}_{-0.0052}$

R, the acoustic scale ℓ_A and the baryon density $\Omega_b^{(0)}h^2$ from Planck15.

The data set is able to constraint the density parameters to a satisfactory level. We see from Fig. (5.2) that the baryons and CDM are anti-correlated, which is expected since both affect the expansion in a similar fashion.

The best-fit value of h results in a H_0 much lower than the local value of H_0, by 2.9σ. The slightly positive values of β indicate an overall energy transfer from dark energy to dark matter, consistent with the thermodynamic considerations [72, 153], but the data is compatible with vanishing coupling, within 1σ. From the marginalized 1-D plot of w_0 we see that it resembles a one-tailed distribution, which is a hint that the data might prefer $w_0 < -1$, that is, a phantom field. As we will shortly see, the preference for w_0 smaller than -1 seems to be a recurring feature of DE models.

In Fig. (5.3) we present the global best-fit curves for the late-time data sets used in this work. The blue lines were computed using the best-fit parameters presented in Tab. (5.8). Lower panels show the residues of the data with respect to the best fit.

A comparison between our constraints on the parameters of all the models analyzed here is presented in Tab. (5.9). Since we sampled the chains for each DE model under roughly the same general assumptions and using exactly the same data set, we diminish any systematics in the comparison between candidates, blaming any differences on the

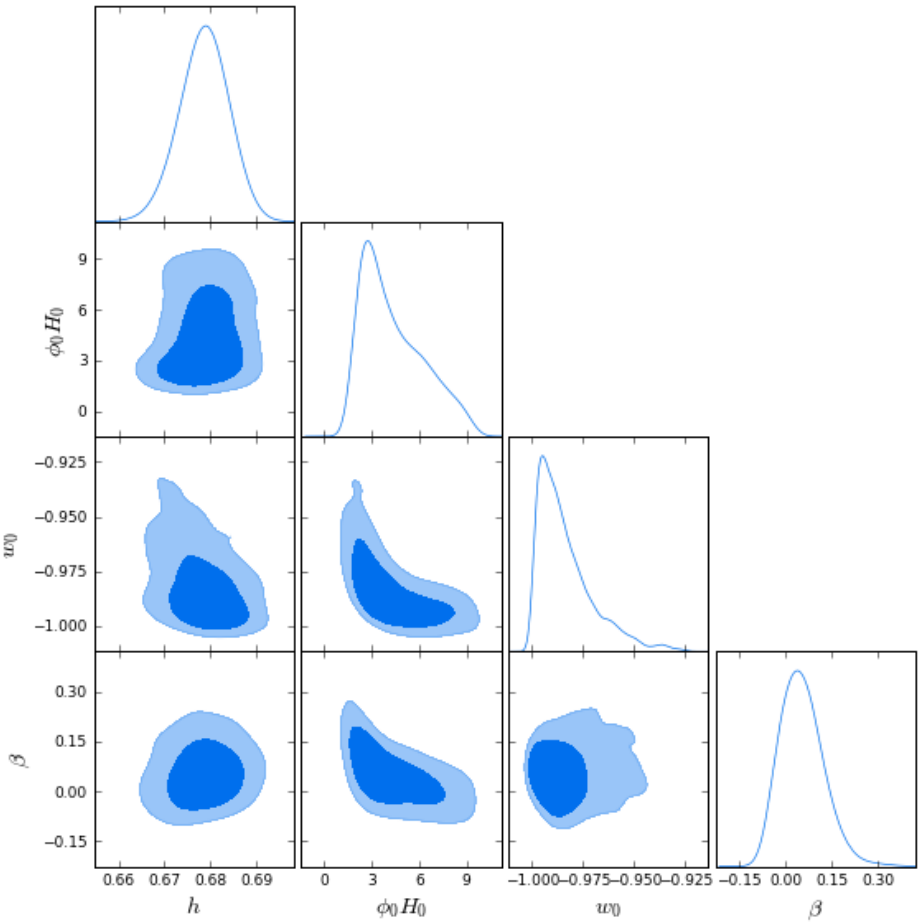

Figure 5.1: Posterior distribution of h and the scalar field parameters for the tachyonic model. The contour plots on each panel are shown at 68% and 95% confidence level.

intrinsic properties of the models.

We note that all the parameters are compatible with each other. As previously stated, the other 3 models where w_0 is fitted along with the other parameters, wCDM and both IDE models, prefer $w_0 < -1$. Another common feature is H_0 significantly lower than the local measurement, but the tension is higher for the tachyon model. Note also that, contrary to the ITM case, the IDE1 and IDE2 models prefer negative values for the coupling constant, but still compatible with zero.

As far as the best-fit parameters are concerned, all the dynamical dark energy models considered is this work are compatible with the standard ΛCDM model.

Now we turn our attention to the information criteria. In Tab. 5.10 we present the values of χ^2, ΔAIC and ΔBIC for the five analyzed models.

The model that best fits the observational set is IDE1. In fact, as far as the

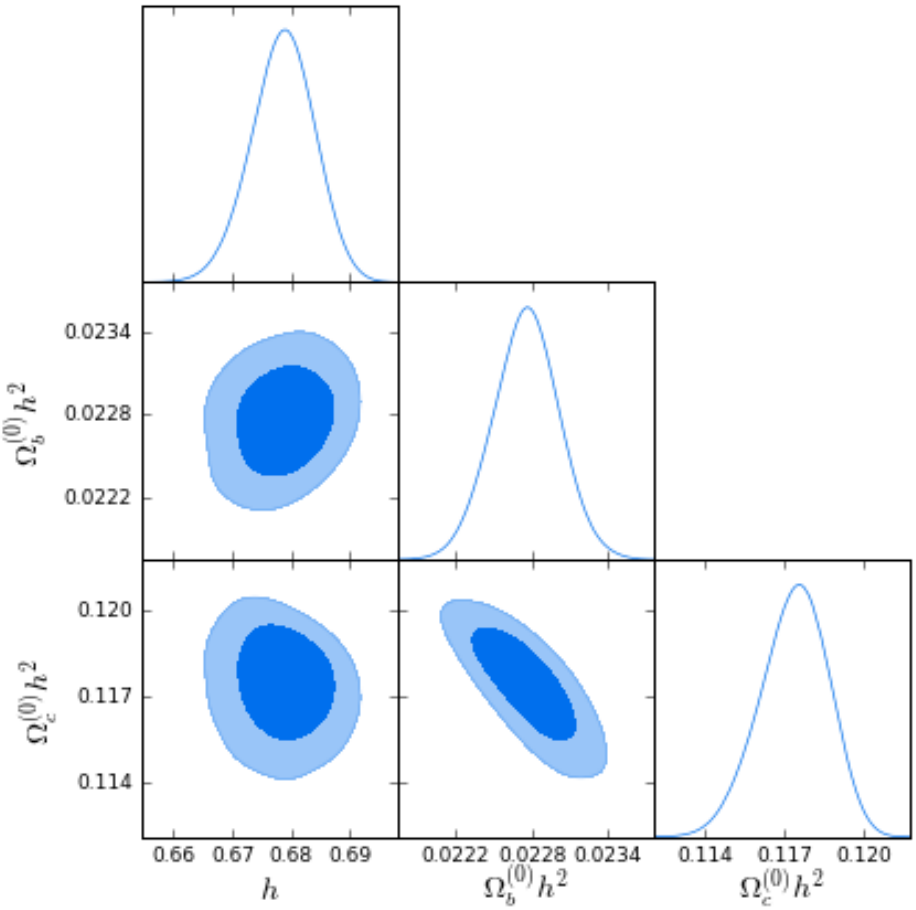

Figure 5.2: Posterior distribution of h the density parameters for the tachyonic model. The contour plots on each panel are shown at 68% and 95% confidence level.

minimum chi-squared is concerned, all models but ITM fits the data better than the concordance ΛCDM. That is not a surprise since, as noted above, the additional degrees of freedom usually results in a lower χ^2. But only usually: the tachyon model is not able to reproduce the collection of data points as well as its counterparts, despite the fact that it is the candidate with the largest number of free parameters.

The resulting chi-squared does not paint the whole picture, though. According to the Akaike criterion, wCDM is the best dark energy model, hence we adopted it as the reference. IDE1 comes in a close second, still better than ΛCDM. Despite its ability to fit the observations slightly better than the concordance model, the extra parameters in IDE2 make the models less appealing. Naturally, due to its higher chi-squared combined with the additional degrees of freedom, ITM has the worst AIC. Assuming that wCDM is the right dark energy paradigm, both ΛCDM and IDE1 have strong

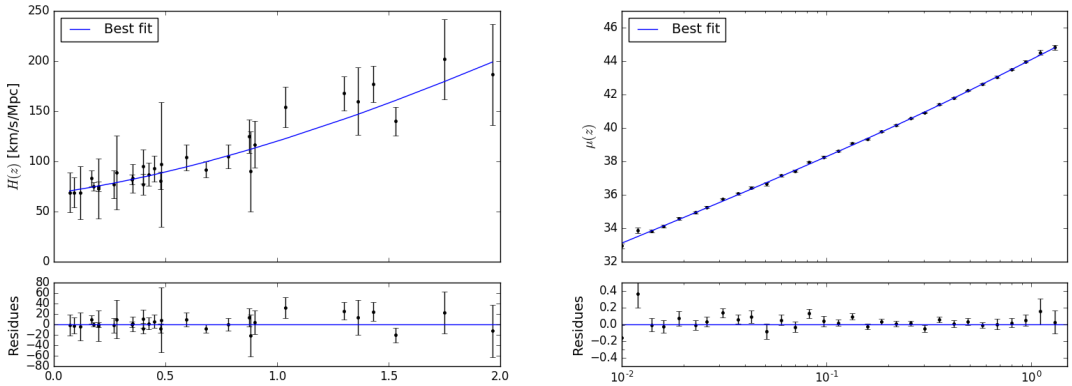

(a) CC. (b) SNe.

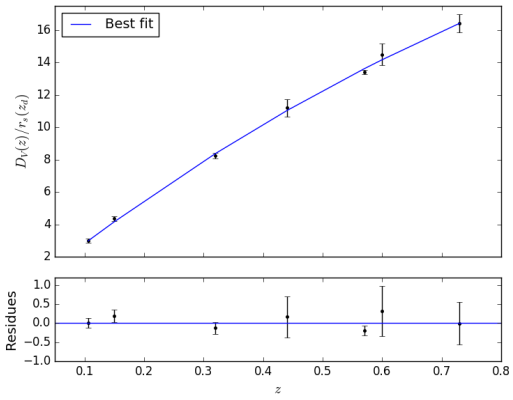

(c) BAO.

Figure 5.3: Late-time expansion history dataset used in this work. The blue lines were computed using the best-fit parameters presented in Table (5.8). Lower panels show the residues of the data with respect to the best fit.

support from the reference model, $IDE2$ has moderate support, and the ITM has barely any. By the same token, if we adopt ΛCDM as reference the conclusion does not change significantly. The new relative differences are: $\Delta AIC(IDE1) = -0.95$, $\Delta AIC(IDE2) = 3.32$, $\Delta AIC(ITM) = 7.67$. The interacting tachyon becomes slightly more appealing, but not as competitive as the alternatives.

The picture changes a little when the importance of the penalty term is enhanced. The Bayesian criterion favors the ΛCDM model and its lack of additional parameters, followed by wCDM, IDE1, IDE2, and ITM, respectively. wCDM shows strong support from the concordance model. IDE1 has moderate support, due to the enhanced complexity factor. IDE2 has significantly less support, while the tachyonic candidate has no support at all.

Table 5.9: Best-fit values and marginalized constraints on the nuisance parameter M and on the cosmological parameters h, $\Omega_b^{(0)}h^2$, $\Omega_c^{(0)}h^2$, w_0 and β at 68% confidence level for all DE models analyzed in this work. When the upper and lower limits are equal we report the uncertainty in the last digits by the numbers between parentheses, corresponding to one standard deviation.

Parameter	ΛCDM	wCDM	IDE1	IDE2	Tachyon
M	$24.952^{0.021}_{-0.020}$	$24.962^{0.023}_{-0.025}$	$24.959^{0.025}_{-0.024}$	24.961(24)	$24.955^{0.023}_{-0.022}$
h	0.6840(42)	$0.6896^{0.0087}_{-0.0086}$	0.6922(88)	0.6924(87)	$0.6787^{0.0056}_{-0.0051}$
$\Omega_b^{(0)}h^2$	0.02237(14)	0.02232(15)	0.02262(29)	0.02240(16)	0.02276(26)
$\Omega_c^{(0)}h^2$	$0.12005^{0.00048}_{-0.00049}$	0.12042(69)	0.1183(16)	$0.11975^{0.00087}_{-0.00086}$	$0.1174^{0.0014}_{-0.0012}$
w_0	-	−1.03(4)	−1.067(50)	−1.064(47)	$-0.984^{0.005}_{-0.016}$
β	-	-	−0.0086(61)	−0.0019(16)	$0.053^{0.058}_{-0.079}$

Table 5.10: Summary of the information criteria results. Here k stands for the number of fitted parameters, which is the sum of the JLA nuisance parameter M and the cosmological parameter of each model. The reference model in the Akaike criterion is wCDM. For the Bayesian criterion, we used ΛCDM as reference.

Model	χ^2_{min}	k	ΔAIC	ΔBIC
ΛCDM	76.34	4	1.97	**0**
wCDM	72.37	5	**0**	0.34
IDE1	**71.89**	6	1.02	3.66
IDE2	75.66	6	5.29	7.93
Tachyon	78.00	7	9.63	14.58

Hence, according to this analysis, the ΛCDM and wCDM paradigms are on equal footing as far as the expansion history of the universe can tell. The coupled DE model with coupling proportional to ρ_{de}, also known as IDE1, is a strong contender, very successful in fitting the observations, but the extra parameters take a toll on the statistical quality. The interacting dark energy model IDE2, with coupling proportional to ρ_c, also reproduce the data very well (in fact, marginally better than ΛCDM) but, again, the additional degrees of freedom reduce the appeal of the model, due to the enhanced complexity. Finally, the interacting tachyon model, which consists of a non-canonical scalar field coupled to dark matter as the source of dark energy, is not an appealing candidate, at least as far as this analysis goes. Despite its theoretical attractiveness, the model was not able to fit the data as well as its counterparts and, due to the extra degrees of freedom, it is harshly punished when the information criteria are employed.

Chapter 6

Conclusion

In this work, we studied dark energy models, mainly those different from the standard cosmological constant. The main objective was to test a model with an interaction between dark energy and dark matter, where DE would be a tachyon scalar field, in an FLRW background. With that in mind, we compared the theoretical predictions of the model with some of the most recent observational data available, namely, direct measurements of the Hubble parameter, the luminous distance of supernovae, baryon acoustic oscillations, CMB anisotropy and local measurements of the Hubble constant. To assess how well the interacting tachyon model fits into the cosmological scenario, we compare its results with those of other dark energy candidates.

In Chapter 2 we developed the necessary cosmological basis for the discussion in the following chapters. The observational evidence of accelerated expansion was presented in Chapter 3, where we also introduced some potential candidates for dark energy. In Chapter 4 we approached the cosmological properties of the tachyon scalar field and presented our proposed coupled model, the ITM. Finally, in Chapter 5, we explain the methodology and the data set used in the parameter extraction, as well as the comparison between the models. We developed a numerical code that solves the background equations and extracts the cosmological parameters with the help of an MCMC engine widely used in the literature.

We conclude that the tachyon scalar field is an interesting candidate for dark energy from a theoretical point of view since it is the low-energy limit of a more fundamental

theory. Indeed, it can explain the observational data and has interesting cosmological properties. Like other coupled scalar field models, the ITM parameters are degenerated, to a certain degree. Although cosmologically feasible, it cannot explain the observational facts as well as other, simpler, dark energy models. Such difficulty was found both from the point of view of the accuracy-of-fit and the complexity given by the number of degrees of freedom of the model.

As to the possible paths to be followed, the most natural one would be to analyze the health of the model in linear perturbation theory, in particular with regard to the structure formation in the universe. Because the tachyon scalar field behaves like dust at high redshifts, it is possible that it will cluster. It would be interesting to know how such a clustering would behave and whether it would still be possible to realize the late-time accelerated cosmological solution. To do so, the perturbed equations should be implemented in one of the available Boltzmann codes, such as `CAMB` [1] or `CLASS` [2]. Thus it would be possible to compare the theoretical predictions with information on the growth of structure, such as $f\sigma_8$ measurements, and also with the full CMB likelihood. Certainly, such an analysis would bring much more information about the model, imposing more robust constraints on the tachyon interacting scalar field.

[1] `http://camb.info/`
[2] `http://class-code.net/`

Bibliography

[1] A. Zee, *Einstein gravity in a nutshell*. Princeton University Press, Princeton, 2013.

[2] S. Carroll, *Spacetime and geometry : an introduction to general relativity*. Addison Wesley, San Francisco, 2004.

[3] S. Dodelson, *Modern cosmology*. Academic Press, An Imprint of Elsevier, San Diego, California, 2003.

[4] Planck collaboration, P. A. R. Ade et al., *Planck 2015 results. XIII. Cosmological parameters*, *Astron. Astrophys.* **594** (2016) A13, [1502.01589].

[5] D. Gorbunov, *Introduction to the theory of the early universe : cosmological perturbations and inflationary theory*. World Scientific, Singapore Hackensack, N.J, 2011.

[6] D. J. Fixsen, E. S. Cheng, J. M. Gales, J. C. Mather, R. A. Shafer and E. L. Wright, *The Cosmic Microwave Background spectrum from the full COBE FIRAS data set*, *Astrophys. J.* **473** (1996) 576, [astro-ph/9605054].

[7] D. J. Fixsen, *The Temperature of the Cosmic Microwave Background*, *Astrophys. J.* **707** (Dec., 2009) 916–920, [0911.1955].

[8] G. Bertone, *Particle dark matter : observations, models and searches*. Cambridge University Press, Cambridge, UK New York, 2010.

[9] D. H. Weinberg, M. J. Mortonson, D. J. Eisenstein, C. Hirata, A. G. Riess and E. Rozo, *Observational Probes of Cosmic Acceleration*, *Phys. Rept.* **530** (2013) 87–255, [1201.2434].

[10] C.-P. Ma and E. Bertschinger, *Cosmological perturbation theory in the synchronous and conformal Newtonian gauges*, *Astrophys. J.* **455** (1995) 7–25, [astro-ph/9506072].

[11] A. G. Riess et al., *A 2.4% Determination of the Local Value of the Hubble Constant*, *Astrophys. J.* **826** (2016) 56, [1604.01424].

[12] E. Carretta, R. G. Gratton, G. Clementini and F. Fusi Pecci, *Distances, ages and epoch of formation of globular clusters*, *Astrophys. J.* **533** (2000) 215–235, [astro-ph/9902086].

[13] R. Jimenez, P. Thejll, U. Jorgensen, J. MacDonald and B. Pagel, *Ages of globular clusters: a new approach*, *Mon. Not. Roy. Astron. Soc.* **282** (1996) 926–942, [astro-ph/9602132].

[14] B. M. S. Hansen, J. Brewer, G. G. Fahlman, B. K. Gibson, R. Ibata, M. Limongi et al., *The white dwarf cooling sequence of the globular cluster messier 4*, *Astrophys. J.* **574** (2002) L155–L158, [astro-ph/0205087].

[15] Supernova Search Team collaboration, A. G. Riess et al., *Observational evidence from supernovae for an accelerating universe and a cosmological constant*, *Astron. J.* **116** (1998) 1009–1038, [astro-ph/9805201].

[16] Supernova Cosmology Project collaboration, S. Perlmutter et al., *Measurements of Omega and Lambda from 42 high redshift supernovae*, *Astrophys. J.* **517** (1999) 565–586, [astro-ph/9812133].

[17] L. Amendola and S. Tsujikawa, *Dark energy : theory and observations*. Cambridge University Press, New York, 2010.

[18] W. Hillebrandt and J. C. Niemeyer, *Type Ia supernova explosion models*, *Ann. Rev. Astron. Astrophys.* **38** (2000) 191–230, [astro-ph/0006305].

[19] SDSS collaboration, M. Betoule et al., *Improved cosmological constraints from a joint analysis of the SDSS-II and SNLS supernova samples*, *Astron. Astrophys.* **568** (2014) A22, [1401.4064].

[20] A. A. Penzias and R. W. Wilson, *A Measurement of excess antenna temperature at 4080-Mc/s*, *Astrophys. J.* **142** (1965) 419–421.

[21] S. Weinberg, *Cosmology*. Oxford University Press, Oxford New York, 2008.

[22] V. F. Mukhanov, *Physical foundations of cosmology*. Cambridge University Press, Cambridge, UK New York, 2005.

[23] W. Hu and N. Sugiyama, *Small scale cosmological perturbations: An Analytic approach*, *Astrophys. J.* **471** (1996) 542–570, [astro-ph/9510117].

[24] Y. Wang and P. Mukherjee, *Observational Constraints on Dark Energy and Cosmic Curvature*, *Phys. Rev.* **D76** (2007) 103533, [astro-ph/0703780].

[25] J. R. Bond, G. Efstathiou and M. Tegmark, *Forecasting cosmic parameter errors from microwave background anisotropy experiments*, *Mon. Not. Roy. Astron. Soc.* **291** (1997) L33–L41, [astro-ph/9702100].

[26] G. Efstathiou and J. R. Bond, *Cosmic confusion: Degeneracies among cosmological parameters derived from measurements of microwave background anisotropies*, *Mon. Not. Roy. Astron. Soc.* **304** (1999) 75–97, [astro-ph/9807103].

[27] WMAP collaboration, E. Komatsu et al., *Seven-Year Wilkinson Microwave Anisotropy Probe (WMAP) Observations: Cosmological Interpretation*, *Astrophys. J. Suppl.* **192** (2011) 18, [1001.4538].

[28] SDSS collaboration, D. J. Eisenstein et al., *Detection of the baryon acoustic peak in the large-scale correlation function of SDSS luminous red galaxies*, *Astrophys. J.* **633** (2005) 560–574, [astro-ph/0501171].

[29] B. A. Bassett and R. Hlozek, *Baryon Acoustic Oscillations*, 0910.5224.

[30] D. J. Eisenstein and W. Hu, *Baryonic features in the matter transfer function*, *Astrophys. J.* **496** (1998) 605, [astro-ph/9709112].

[31] Planck collaboration, P. A. R. Ade et al., *Planck 2015 results. XIV. Dark energy and modified gravity*, 1502.01590.

[32] S. Weinberg, *The Cosmological Constant Problem*, *Rev. Mod. Phys.* **61** (1989) 1–23.

[33] S. M. Carroll, *The Cosmological constant*, *Living Rev. Rel.* **4** (2001) 1, [astro-ph/0004075].

[34] A. Einstein, *The Foundation of the General Theory of Relativity*, *Annalen Phys.* **49** (1916) 769–822.

[35] A. Einstein, *Cosmological Considerations in the General Theory of Relativity*, *Sitzungsber. Preuss. Akad. Wiss. Berlin (Math. Phys.)* **1917** (1917) 142–152.

[36] E. Hubble, *A relation between distance and radial velocity among extra-galactic nebulae*, *Proceedings of the National Academy of Sciences* **15** (1929) 168–173.

[37] P. Astier, *Can luminosity distance measurements probe the equation of state of dark energy*, *Phys. Lett.* **B500** (2001) 8–15, [astro-ph/0008306].

[38] D. Huterer and M. S. Turner, *Probing the dark energy: Methods and strategies*, *Phys. Rev.* **D64** (2001) 123527, [astro-ph/0012510].

[39] J. Weller and A. Albrecht, *Future supernovae observations as a probe of dark energy*, *Phys. Rev.* **D65** (2002) 103512, [astro-ph/0106079].

[40] M. Chevallier and D. Polarski, *Accelerating universes with scaling dark matter*, *Int. J. Mod. Phys.* **D10** (2001) 213–224, [gr-qc/0009008].

[41] E. V. Linder, *Exploring the expansion history of the universe*, *Phys. Rev. Lett.* **90** (2003) 091301, [astro-ph/0208512].

[42] H. K. Jassal, J. S. Bagla and T. Padmanabhan, *WMAP constraints on low redshift evolution of dark energy*, *Mon. Not. Roy. Astron. Soc.* **356** (2005) L11–L16, [astro-ph/0404378].

[43] E. M. Barboza, Jr. and J. S. Alcaniz, *A parametric model for dark energy*, *Phys. Lett.* **B666** (2008) 415–419, [0805.1713].

[44] C. Armendariz-Picon, T. Damour and V. F. Mukhanov, *k - inflation*, *Phys. Lett.* **B458** (1999) 209–218, [hep-th/9904075].

[45] L. Amendola et al., *Cosmology and Fundamental Physics with the Euclid Satellite*, 1606.00180.

[46] J. Garriga and V. F. Mukhanov, *Perturbations in k-inflation*, *Phys. Lett.* **B458** (1999) 219–225, [hep-th/9904176].

[47] R. R. Caldwell, R. Dave and P. J. Steinhardt, *Cosmological imprint of an energy component with general equation of state*, *Phys. Rev. Lett.* **80** (1998) 1582–1585, [astro-ph/9708069].

[48] B. Ratra and P. J. E. Peebles, *Cosmological Consequences of a Rolling Homogeneous Scalar Field*, *Phys. Rev.* **D37** (1988) 3406.

[49] E. J. Copeland, A. R. Liddle and D. Wands, *Exponential potentials and cosmological scaling solutions*, *Phys. Rev.* **D57** (1998) 4686–4690, [gr-qc/9711068].

[50] P. J. Steinhardt, L.-M. Wang and I. Zlatev, *Cosmological tracking solutions*, *Phys. Rev.* **D59** (1999) 123504, [astro-ph/9812313].

[51] R. R. Caldwell and E. V. Linder, *The Limits of quintessence*, *Phys. Rev. Lett.* **95** (2005) 141301, [astro-ph/0505494].

[52] I. Zlatev, L.-M. Wang and P. J. Steinhardt, *Quintessence, cosmic coincidence, and the cosmological constant*, *Phys. Rev. Lett.* **82** (1999) 896–899, [astro-ph/9807002].

[53] J. A. Frieman, C. T. Hill, A. Stebbins and I. Waga, *Cosmology with ultralight pseudo Nambu-Goldstone bosons*, *Phys. Rev. Lett.* **75** (1995) 2077–2080, [astro-ph/9505060].

[54] K. Bamba, S. Capozziello, S. Nojiri and S. D. Odintsov, *Dark energy cosmology: the equivalent description via different theoretical models and cosmography tests*, *Astrophys. Space Sci.* **342** (2012) 155–228, [1205.3421].

[55] T. Chiba, A. De Felice and S. Tsujikawa, *Observational constraints on quintessence: thawing, tracker, and scaling models*, *Phys. Rev.* **D87** (2013) 083505, [1210.3859].

[56] S. Tsujikawa, *Quintessence: A Review*, *Class. Quant. Grav.* **30** (2013) 214003, [1304.1961].

[57] A. Sen, *Tachyons in string theory*, *Annales Henri Poincaré* **4** (2003) 31–42.

[58] A. Sen, *Field theory of tachyon matter*, *Mod. Phys. Lett.* **A17** (2002) 1797–1804, [hep-th/0204143].

[59] T. Chiba, T. Okabe and M. Yamaguchi, *Kinetically driven quintessence*, *Phys. Rev.* **D62** (2000) 023511, [astro-ph/9912463].

[60] C. Armendariz-Picon, V. F. Mukhanov and P. J. Steinhardt, *Essentials of k essence*, *Phys. Rev.* **D63** (2001) 103510, [astro-ph/0006373].

[61] M. Gasperini and G. Veneziano, *The Pre - big bang scenario in string cosmology*, *Phys. Rept.* **373** (2003) 1–212, [hep-th/0207130].

[62] F. Piazza and S. Tsujikawa, *Dilatonic ghost condensate as dark energy*, *JCAP* **0407** (2004) 004, [hep-th/0405054].

[63] T. Clifton, P. G. Ferreira, A. Padilla and C. Skordis, *Modified Gravity and Cosmology*, *Phys. Rept.* **513** (2012) 1–189, [1106.2476].

[64] J. Martin and M. Yamaguchi, *DBI-essence*, *Phys. Rev.* **D77** (2008) 123508, [0801.3375].

[65] E. J. Copeland, S. Mizuno and M. Shaeri, *Cosmological Dynamics of a Dirac-Born-Infeld field*, *Phys. Rev.* **D81** (2010) 123501, [1003.2881].

[66] P. F. Gonzalez-Diaz, *K-essential phantom energy: Doomsday around the corner?*, *Phys. Lett.* **B586** (2004) 1–4, [astro-ph/0312579].

[67] R. J. Scherrer, *Purely kinetic k-essence as unified dark matter*, *Phys. Rev. Lett.* **93** (2004) 011301, [astro-ph/0402316].

[68] T. Chiba, *Tracking K-essence*, *Phys. Rev.* **D66** (2002) 063514, [astro-ph/0206298].

[69] S. C. C. Ng, N. J. Nunes and F. Rosati, *Applications of scalar attractor solutions to cosmology*, *Phys. Rev.* **D64** (2001) 083510, [astro-ph/0107321].

[70] T. Barreiro, E. J. Copeland and N. J. Nunes, *Quintessence arising from exponential potentials*, *Phys. Rev.* **D61** (2000) 127301, [astro-ph/9910214].

[71] V. Sahni and L.-M. Wang, *A New cosmological model of quintessence and dark matter*, *Phys. Rev.* **D62** (2000) 103517, [astro-ph/9910097].

[72] B. Wang, E. Abdalla, F. Atrio-Barandela and D. Pavon, *Dark Matter and Dark Energy Interactions: Theoretical Challenges, Cosmological Implications and Observational Signatures*, *Rept. Prog. Phys.* **79** (2016) 096901, [1603.08299].

[73] J. M. Aguirregabiria and R. Lazkoz, *Tracking solutions in tachyon cosmology*, *Phys. Rev.* **D69** (2004) 123502, [hep-th/0402190].

[74] E. J. Copeland, M. R. Garousi, M. Sami and S. Tsujikawa, *What is needed of a tachyon if it is to be the dark energy?*, *Phys. Rev.* **D71** (2005) 043003, [hep-th/0411192].

[75] B. Gumjudpai, T. Naskar, M. Sami and S. Tsujikawa, *Coupled dark energy: Towards a general description of the dynamics*, *JCAP* **0506** (2005) 007, [hep-th/0502191].

[76] L. Amendola, M. Quartin, S. Tsujikawa and I. Waga, *Challenges for scaling cosmologies*, *Phys. Rev.* **D74** (2006) 023525, [astro-ph/0605488].

[77] B. Bertotti, L. Iess and P. Tortora, *A test of general relativity using radio links with the cassini spacecraft*, *Nature* **425** (2003) 374–376.

[78] T. Dent, S. Stern and C. Wetterich, *Time variation of fundamental couplings and dynamical dark energy*, *JCAP* **0901** (2009) 038, [0809.4628].

[79] A. W. Brookfield, C. van de Bruck, D. F. Mota and D. Tocchini-Valentini, *Cosmology with massive neutrinos coupled to dark energy*, *Phys. Rev. Lett.* **96** (2006) 061301, [astro-ph/0503349].

[80] S. Ahmad, N. Myrzakulov and R. Myrzakulov, *Tachyon field non-minimally coupled to massive neutrino matter*, *JCAP* **1607** (2016) 032, [1510.04795].

[81] L. Amendola, M. Baldi and C. Wetterich, *Quintessence cosmologies with a growing matter component*, *Phys. Rev.* **D78** (2008) 023015, [0706.3064].

[82] L. Amendola, *Coupled quintessence*, *Phys. Rev.* **D62** (2000) 043511, [astro-ph/9908023].

[83] A. A. Costa, L. C. Olivari and E. Abdalla, *Quintessence with Yukawa Interaction*, *Phys. Rev.* **D92** (2015) 103501, [1411.3660].

[84] A. B. Pavan, E. G. M. Ferreira, S. Micheletti, J. C. C. de Souza and E. Abdalla, *Exact cosmological solutions of models with an interacting dark sector*, *Phys. Rev.* **D86** (2012) 103521, [1111.6526].

[85] S. Micheletti, E. Abdalla and B. Wang, *A Field Theory Model for Dark Matter and Dark Energy in Interaction*, *Phys. Rev.* **D79** (2009) 123506, [0902.0318].

[86] A. A. Costa, X.-D. Xu, B. Wang, E. G. M. Ferreira and E. Abdalla, *Testing the Interaction between Dark Energy and Dark Matter with Planck Data*, *Phys. Rev.* **D89** (2014) 103531, [1311.7380].

[87] A. A. Costa, X.-D. Xu, B. Wang and E. Abdalla, *Constraints on interacting dark energy models from Planck 2015 and redshift-space distortion data*, 1605.04138.

[88] R. J. F. Marcondes, R. C. G. Landim, A. A. Costa, B. Wang and E. Abdalla, *Analytic study of the effect of dark energy-dark matter interaction on the growth of structures*, *JCAP* **1612** (2016) 009, [1605.05264].

[89] D. Pavon and W. Zimdahl, *Holographic dark energy and cosmic coincidence*, *Phys. Lett.* **B628** (2005) 206–210, [gr-qc/0505020].

[90] B. Wang, J. Zang, C.-Y. Lin, E. Abdalla and S. Micheletti, *Interacting Dark Energy and Dark Matter: Observational Constraints from Cosmological Parameters*, *Nucl. Phys.* **B778** (2007) 69–84, [astro-ph/0607126].

[91] W. Zimdahl and D. Pavon, *Interacting holographic dark energy*, *Class. Quant. Grav.* **24** (2007) 5461–5478, [astro-ph/0606555].

[92] L. Amendola, V. Pettorino, C. Quercellini and A. Vollmer, *Testing coupled dark energy with next-generation large-scale observations*, *Phys. Rev.* **D85** (2012) 103008, [1111.1404].

[93] L. Amendola, G. Camargo Campos and R. Rosenfeld, *Consequences of dark matter-dark energy interaction on cosmological parameters derived from SNIa data*, *Phys. Rev.* **D75** (2007) 083506, [astro-ph/0610806].

[94] C. Feng, B. Wang, E. Abdalla and R.-K. Su, *Observational constraints on the dark energy and dark matter mutual coupling*, *Phys. Lett.* **B665** (2008) 111–119, [0804.0110].

[95] J.-H. He, B. Wang and E. Abdalla, *Testing the interaction between dark energy and dark matter via latest observations*, *Phys. Rev.* **D83** (2011) 063515, [1012.3904].

[96] J.-H. He, B. Wang and E. Abdalla, *Stability of the curvature perturbation in dark sectors' mutual interacting models*, *Phys. Lett.* **B671** (2009) 139–145, [0807.3471].

[97] J.-H. He and B. Wang, *Effects of the interaction between dark energy and dark matter on cosmological parameters*, *JCAP* **0806** (2008) 010, [0801.4233].

[98] M. R. Garousi, *Tachyon couplings on nonBPS D-branes and Dirac-Born-Infeld action*, *Nucl. Phys.* **B584** (2000) 284–299, [hep-th/0003122].

[99] A. Sen, *Stable nonBPS bound states of BPS D-branes*, *JHEP* **08** (1998) 010, [hep-th/9805019].

[100] A. Sen, *Tachyon condensation on the brane anti-brane system*, *JHEP* **08** (1998) 012, [hep-th/9805170].

[101] B. Zwiebach, *A first course in string theory*. Cambridge University Press, Cambridge New York, 2009.

[102] A. Sen, *Tachyon matter*, *JHEP* **07** (2002) 065, [hep-th/0203265].

[103] A. Sen, *Rolling tachyon*, *JHEP* **04** (2002) 048, [hep-th/0203211].

[104] A. V. Frolov, L. Kofman and A. A. Starobinsky, *Prospects and problems of tachyon matter cosmology*, *Phys. Lett.* **B545** (2002) 8–16, [hep-th/0204187].

[105] T. Padmanabhan and T. R. Choudhury, *Can the clustered dark matter and the smooth dark energy arise from the same scalar field?*, *Phys. Rev.* **D66** (2002) 081301, [hep-th/0205055].

[106] G. Shiu and I. Wasserman, *Cosmological constraints on tachyon matter*, *Phys. Lett.* **B541** (2002) 6–15, [hep-th/0205003].

[107] J. S. Bagla, H. K. Jassal and T. Padmanabhan, *Cosmology with tachyon field as dark energy*, *Phys. Rev.* **D67** (2003) 063504, [astro-ph/0212198].

[108] G. W. Gibbons, *Cosmological evolution of the rolling tachyon*, *Phys. Lett.* **B537** (2002) 1–4, [hep-th/0204008].

[109] T. Padmanabhan, *Accelerated expansion of the universe driven by tachyonic matter*, *Phys. Rev.* **D66** (2002) 021301, [hep-th/0204150].

[110] L. R. W. Abramo and F. Finelli, *Cosmological dynamics of the tachyon with an inverse power-law potential*, *Phys. Lett.* **B575** (2003) 165–171, [astro-ph/0307208].

[111] Z.-K. Guo and Y.-Z. Zhang, *Cosmology with a variable Chaplygin gas*, *Phys. Lett.* **B645** (2007) 326–329, [astro-ph/0506091].

[112] M. Makler, S. Quinet de Oliveira and I. Waga, *Constraints on the generalized Chaplygin gas from supernovae observations*, *Phys. Lett.* **B555** (2003) 1, [astro-ph/0209486].

[113] A. Yu. Kamenshchik, U. Moschella and V. Pasquier, *An Alternative to quintessence*, *Phys. Lett.* **B511** (2001) 265–268, [gr-qc/0103004].

[114] M. C. Bento, O. Bertolami and A. A. Sen, *Generalized Chaplygin gas, accelerated expansion and dark energy matter unification*, *Phys. Rev.* **D66** (2002) 043507, [gr-qc/0202064].

[115] D. Carturan and F. Finelli, *Cosmological effects of a class of fluid dark energy models*, *Phys. Rev.* **D68** (2003) 103501, [astro-ph/0211626].

[116] D. Bertacca, N. Bartolo, A. Diaferio and S. Matarrese, *How the Scalar Field of Unified Dark Matter Models Can Cluster*, *JCAP* **0810** (2008) 023, [0807.1020].

[117] J. C. Fabris, S. V. B. Goncalves and P. E. de Souza, *Density perturbations in a universe dominated by the Chaplygin gas*, *Gen. Rel. Grav.* **34** (2002) 53–63, [gr-qc/0103083].

[118] V. Gorini, A. Y. Kamenshchik, U. Moschella, O. F. Piattella and A. A. Starobinsky, *Gauge-invariant analysis of perturbations in Chaplygin gas unified models of dark matter and dark energy*, *JCAP* **0802** (2008) 016, [0711.4242].

[119] H. Sandvik, M. Tegmark, M. Zaldarriaga and I. Waga, *The end of unified dark matter?*, *Phys. Rev.* **D69** (2004) 123524, [astro-ph/0212114].

[120] L. Amendola, F. Finelli, C. Burigana and D. Carturan, *WMAP and the generalized Chaplygin gas*, *JCAP* **0307** (2003) 005, [astro-ph/0304325].

[121] M. d. C. Bento, O. Bertolami and A. A. Sen, *Generalized Chaplygin gas and CMBR constraints*, *Phys. Rev.* **D67** (2003) 063003, [astro-ph/0210468].

[122] N. Bilic, G. B. Tupper and R. D. Viollier, *Unification of dark matter and dark energy: The Inhomogeneous Chaplygin gas*, *Phys. Lett.* **B535** (2002) 17–21, [astro-ph/0111325].

[123] N. Bilic, G. B. Tupper and R. D. Viollier, *Cosmological tachyon condensation*, *Phys. Rev.* **D80** (2009) 023515, [0809.0375].

[124] D. Bertacca, S. Matarrese and M. Pietroni, *Unified Dark Matter in Scalar Field Cosmologies*, *Mod. Phys. Lett.* **A22** (2007) 2893–2907, [astro-ph/0703259].

[125] N. Bilic, G. B. Tupper and R. D. Viollier, *Chaplygin Gas Cosmology: Unification of Dark Matter and Dark Energy*, *J. Phys.* **A40** (2007) 6877–6882, [gr-qc/0610104].

[126] N. Bilic, G. B. Tupper and R. D. Viollier, *Cosmological k-essence condensation*, in *Physics beyond the standard models of particles, cosmology and astrophysics. Proceedings, 5th International Conference, Beyond 2010, Cape Town, South Africa, February 1-6, 2010*, pp. 503–510, 2011. 1004.3141. DOI.

[127] E. J. Copeland, M. Sami and S. Tsujikawa, *Dynamics of dark energy*, *Int. J. Mod. Phys.* **D15** (2006) 1753–1936, [hep-th/0603057].

[128] A. Feinstein, *Power law inflation from the rolling tachyon*, *Phys. Rev.* **D66** (2002) 063511, [hep-th/0204140].

[129] D. Bazeia, C. B. Gomes, L. Losano and R. Menezes, *First-order formalism and dark energy*, *Phys. Lett.* **B633** (2006) 415–419, [astro-ph/0512197].

[130] R. Trotta, *Bayes in the sky: Bayesian inference and model selection in cosmology*, *Contemp. Phys.* **49** (2008) 71–104, [0803.4089].

[131] D. S. Sivia, *Data analysis : a Bayesian tutorial*. Oxford University Press, Oxford New York, 2006.

[132] R. Trotta, *Bayesian Methods in Cosmology*, 2017. 1701.01467.

[133] D. MacKay, *Information theory, inference, and learning algorithms*. Cambridge University Press, Cambridge, UK New York, 2003.

[134] H. Akaike, *A new look at the statistical model identification*, *IEEE Transactions on Automatic Control* **19** (1974) .

[135] G. Schwarz, *Estimating the dimension of a model*, *Annals of Statistics* **6** (1978) .

[136] A. de la Cruz-Dombriz, P. K. S. Dunsby, O. Luongo and L. Reverberi, *Model-independent limits and constraints on extended theories of gravity from cosmic reconstruction techniques*, *JCAP* **1612** (2016) .

[137] Y.-Y. Xu and X. Zhang, *Comparison of dark energy models after Planck 2015*, *Eur. Phys. J.* **C76** (2016) 588, [1607.06262].

[138] R. Jimenez and A. Loeb, *Constraining cosmological parameters based on relative galaxy ages*, *Astrophys. J.* **573** (2002) 37–42, [astro-ph/0106145].

[139] M. Moresco, R. Jimenez, L. Verde, A. Cimatti, L. Pozzetti, C. Maraston et al., *Constraining the time evolution of dark energy, curvature and neutrino properties with cosmic chronometers*, *JCAP* **2016** (2016) 039, [1604.00183].

[140] M. Moresco et al., *Improved constraints on the expansion rate of the Universe up to $z \sim 1.1$ from the spectroscopic evolution of cosmic chronometers*, *JCAP* **1208** (2012) 006, [1201.3609].

[141] M. Moresco, L. Pozzetti, A. Cimatti, R. Jimenez, C. Maraston, L. Verde et al., *A 6% measurement of the Hubble parameter at $z \sim 0.45$: direct evidence of the epoch of cosmic re-acceleration*, *JCAP* **1605** (2016) 014, [1601.01701].

[142] C. Zhang, H. Zhang, S. Yuan, S. Liu, T.-J. Zhang and Y.-C. Sun, *Four new observational h (z) data from luminous red galaxies in the sloan digital sky survey data release seven*, *Research in Astronomy and Astrophysics* **14** (2014) 1221.

[143] R. Jimenez, L. Verde, T. Treu and D. Stern, *Constraints on the equation of state of dark energy and the Hubble constant from stellar ages and the CMB*, *Astrophys. J.* **593** (2003) 622–629, [astro-ph/0302560].

[144] D. Stern, R. Jimenez, L. Verde, M. Kamionkowski and S. A. Stanford, *Cosmic Chronometers: Constraining the Equation of State of Dark Energy. I: H(z) Measurements*, *JCAP* **1002** (2010) 008, [0907.3149].

[145] J. Simon, L. Verde and R. Jimenez, *Constraints on the redshift dependence of the dark energy potential*, *Phys. Rev.* **D71** (2005) 123001, [astro-ph/0412269].

[146] M. Moresco, *Raising the bar: new constraints on the Hubble parameter with cosmic chronometers at z 2*, *Mon. Not. Roy. Astron. Soc.* **450** (2015) L16–L20, [1503.01116].

[147] F. Beutler, C. Blake, M. Colless, D. H. Jones, L. Staveley-Smith, L. Campbell et al., *The 6dF Galaxy Survey: Baryon Acoustic Oscillations and the Local*

Hubble Constant, *Mon. Not. Roy. Astron. Soc.* **416** (2011) 3017–3032, [1106.3366].

[148] A. J. Ross, L. Samushia, C. Howlett, W. J. Percival, A. Burden and M. Manera, *The clustering of the SDSS DR7 main Galaxy sample – I. A 4 per cent distance measure at $z = 0.15$*, *Mon. Not. Roy. Astron. Soc.* **449** (2015) 835–847, [1409.3242].

[149] BOSS collaboration, L. Anderson et al., *The clustering of galaxies in the SDSS-III Baryon Oscillation Spectroscopic Survey: baryon acoustic oscillations in the Data Releases 10 and 11 Galaxy samples*, *Mon. Not. Roy. Astron. Soc.* **441** (2014) 24–62, [1312.4877].

[150] E. A. Kazin et al., *The WiggleZ Dark Energy Survey: improved distance measurements to $z = 1$ with reconstruction of the baryonic acoustic feature*, *Mon. Not. Roy. Astron. Soc.* **441** (2014) 3524–3542, [1401.0358].

[151] D. Foreman-Mackey, D. W. Hogg, D. Lang and J. Goodman, *emcee: The MCMC Hammer*, *Publ. Astron. Soc. Pac.* **125** (2013) 306–312, [1202.3665].

[152] A. Gelman and D. B. Rubin, *Inference from iterative simulation using multiple sequences*, *Statist. Sci.* **7** (11, 1992) 457–472.

[153] B. Wang, C.-Y. Lin, D. Pavon and E. Abdalla, *Thermodynamical description of the interaction between dark energy and dark matter*, *Phys. Lett.* **B662** (2008) 1–6, [0711.2214].